

Replies to Referees

This document contains our replies to referee comments, all the relevant changes made in the manuscript (preceded by DONE), as well as a marked-up version of the revised manuscript.

Reply to Referee #2

Belmonte Rivas et al. report the global NO₂ volume mixing ratio (VMR) profile climatology for cloudy scenes obtained by applying cloud-slicing technique to OMI NO₂ tropospheric column and OMI O₂-O₂ cloud product. They maximize the number of usable OMI measurements by employing cloud radiance fraction (CRF) threshold greater than 20% for individual measurements and 50% for daily representative value for grid boxes. The authors then compare the OMI cloud-slicing profile climatology with TM4 model results, and suggest possible reasons that may have caused the apparent model shortcomings. There are several major and minor points that need to be addressed before publication in ACP.

This reviewer brings forward a number of issues (about the influence of a priori information on results, the analysis of profile errors, and the selection of CRF thresholds) that were not mentioned in the original manuscript in the interest of space. The authors are glad to clarify these topics here in the hopes of satisfying his/her concerns.

Major comments:

1) Contribution of a priori information to the results

From the method presented in the paper, NO₂ volume mixing ratio (VMR) for a pressure bin is proportional to:

$$c \cdot \text{VMR}(p_{\text{mid}}) = \frac{\text{VCD}_{\text{above}}(p_{\text{dn}}) - \text{VCD}_{\text{above}}(p_{\text{up}})}{p_{\text{dn}} - p_{\text{up}}}$$

where p_{mid} is center of the target pressure bin, p_{dn} is lower threshold and p_{up} is the upper threshold of the bin, $\text{VCD}_{\text{above}}$ is tropospheric NO₂ VCD above a given cloud pressure level, and c is a constant. And from Eq. (2) in the paper,

$$c \cdot \text{VMR}(p_{\text{mid}}) = \frac{\frac{\text{SCD}(p_{\text{dn}}) - \text{SCD}_{\text{strat}} - \text{SCD}_{\text{below}}(p_{\text{dn}})}{\text{AMF}_{\text{above}}(p_{\text{dn}})} - \frac{\text{SCD}(p_{\text{up}}) - \text{SCD}_{\text{strat}} - \text{SCD}_{\text{below}}(p_{\text{up}})}{\text{AMF}_{\text{above}}(p_{\text{up}})}}{p_{\text{dn}} - p_{\text{up}}}$$

Here, SCD (no subscript) is the measured NO₂ slant column at a given cloudy scene. (p_{dn}) or (p_{up}) means that the measured cloud pressure is p_{dn} or p_{up} at the given scene where the SCD is measured. SCD_{strat} is stratospheric slant column (VCD_{strat} (from model) * AMF_{strat}), and is independent of the target pressure bin. We may neglect stratospheric SCD in calculating free tropospheric NO₂ VMR since the stratospheric SCD and AMF_{above} do not vary much between p_{dn} and p_{up}.

Note that AMF_{above} may vary appreciably with cloud pressure, particularly for low cloud levels over polluted areas. Cancelling the stratospheric contributions like the reviewer suggests may produce large errors under certain conditions, but let us continue.

According to Eq. (3), SCD_{below} is the integrated model profile from the ground to the cloud pressure weighted by the scattering weight, and then multiplied by (1-CRF). Given this information, VMR(p_{mid}) can be expressed:

$$\begin{aligned} c \cdot \text{VMR}(p_{\text{mid}}) &= \frac{\frac{\text{SCD}(p_{\text{dn}})}{\text{AMF}_{\text{above}}(p_{\text{dn}})} - \frac{\text{SCD}(p_{\text{up}})}{\text{AMF}_{\text{above}}(p_{\text{up}})}}{p_{\text{dn}} - p_{\text{up}}} - \frac{\frac{\text{SCD}_{\text{below}}(p_{\text{dn}})}{\text{AMF}_{\text{above}}(p_{\text{dn}})} - \frac{\text{SCD}_{\text{below}}(p_{\text{up}})}{\text{AMF}_{\text{above}}(p_{\text{up}})}}{p_{\text{dn}} - p_{\text{up}}} \\ &= \frac{\frac{\text{SCD}(p_{\text{dn}})}{\text{AMF}_{\text{above}}(p_{\text{dn}})} - \frac{\text{SCD}(p_{\text{up}})}{\text{AMF}_{\text{above}}(p_{\text{up}})}}{p_{\text{dn}} - p_{\text{up}}} - \frac{\frac{(1-\text{CRF}(p_{\text{dn}})) \int_{p_{\text{sfc}}}^{p_{\text{dn}}} m(p)n(p) dp}{\text{AMF}_{\text{above}}(p_{\text{dn}})} - \frac{(1-\text{CRF}(p_{\text{up}})) \int_{p_{\text{sfc}}}^{p_{\text{up}}} m(p)n(p) dp}{\text{AMF}_{\text{above}}(p_{\text{up}})}}{p_{\text{dn}} - p_{\text{up}}} \end{aligned}$$

where n(p) is the a priori trace gas profile from the model, m(p) is the scattering weight, and p_{sfc} is the surface pressure. Here, the first term consists of the actual contribution from NO₂ between p_{dn} and p_{up}, the true information we are looking for. On the other hand, the second term consists of a priori information of below-cloud NO₂ profile. If CRF and AMF are similar with respect to pressure in (p_{dn}, p_{up}) range, the second term is simply (1-CRF) * n(p_{mid}),

Note that AMF_{above} (mean sensitivity above the cloud) may differ from the mean sensitivity in the cloud (i.e., strictly between p_{dn} and p_{up}), so that approximating the second term by (1-CRF) * n(p_{mid}) may be perilous too, but we understand the reviewer's concerns. Please continue.

Assuming that CRFs and AMFs (above and below the cloud) were similar (which is a very strong assumption, not generally applicable but anyway, stated here as an exercise), then

one would get that the vertical column between cloud levels is equal to the first term, i.e. the difference between vertical columns sensed at two cloud levels (assuming cancellation of the stratospheric component), which we could write as:

$$\begin{aligned} c * \text{VMR}(p_{\text{mid}}) * (p_{\text{dn}} - p_{\text{up}}) &= \text{VCD}_{\text{dn}} - \text{VCD}_{\text{up}} = \\ &= \text{VCD}_{\text{above,dn}} - \text{VCD}_{\text{above,up}} + (1-\text{CRF}) * (\text{VCD}_{\text{below,dn}} - \text{VCD}_{\text{below,up}}) \end{aligned}$$

Where we take roughly:

$$\text{VCD}_{\text{dn}} = \text{VCD}_{\text{above,dn}} + (1-\text{CRF}) * \text{VCD}_{\text{below,dn}}$$

$$\text{VCD}_{\text{up}} = \text{VCD}_{\text{above,up}} + (1-\text{CRF}) * \text{VCD}_{\text{below,up}}$$

Minus the second term, which is the difference between vertical columns sensed below those two cloud levels:

$$(1-\text{CRF}) * (\text{VCD}_{\text{below,dn}} - \text{VCD}_{\text{below,up}}) \quad \dots \text{proportional to } (1-\text{CRF}) * n(p_{\text{mid}})$$

Which is precisely the correction that we seek to remove from the first term. The a priori information is used to correct for what contamination is expected to arise from underneath the cloud. The difference, however, lies in the fact that the a priori correction in Eq.(2) of the manuscript is applied to the tropospheric slant column SCD (not to the tropospheric vertical column VCD): in this case the contaminating term (and its correction) is preceded by a AMFbelow/AMFabove factor which is typically smaller than unity (since the scattering sensitivity $m(z)$ typically decreases towards the surface). There will be contamination from the lower layers in cloud slicing, but this contamination is reduced by the scattering sensitivity profile under the cloud when dealing with SCDs.

the difference of a priori below-cloud columns for p_{dn} and p_{up} times the ratio of the clear portion to the pixel. Since the CRF threshold is not very high (20% for individual measurements and 50% for daily representative value per grid box), the retrieved VMR contains a priori information, but it is not clear exactly how much.

The next figure (Fig.R1) shows the magnitude of the annual mean correction SCDbelow relative to the annual mean corrected slant column (SCDabove = $\text{VCD}_{\text{above}} * \text{AMFabove}$) at 870 hPa in the CRF 50% case. Over strongly polluting urban centers, this quantity may be as high as 100%, meaning that the model based correction is allowed to remove up to 50% of the original total tropospheric slant column (SCD_{tot} = SCD_{above} + SCD_{below})

observed by OMI.

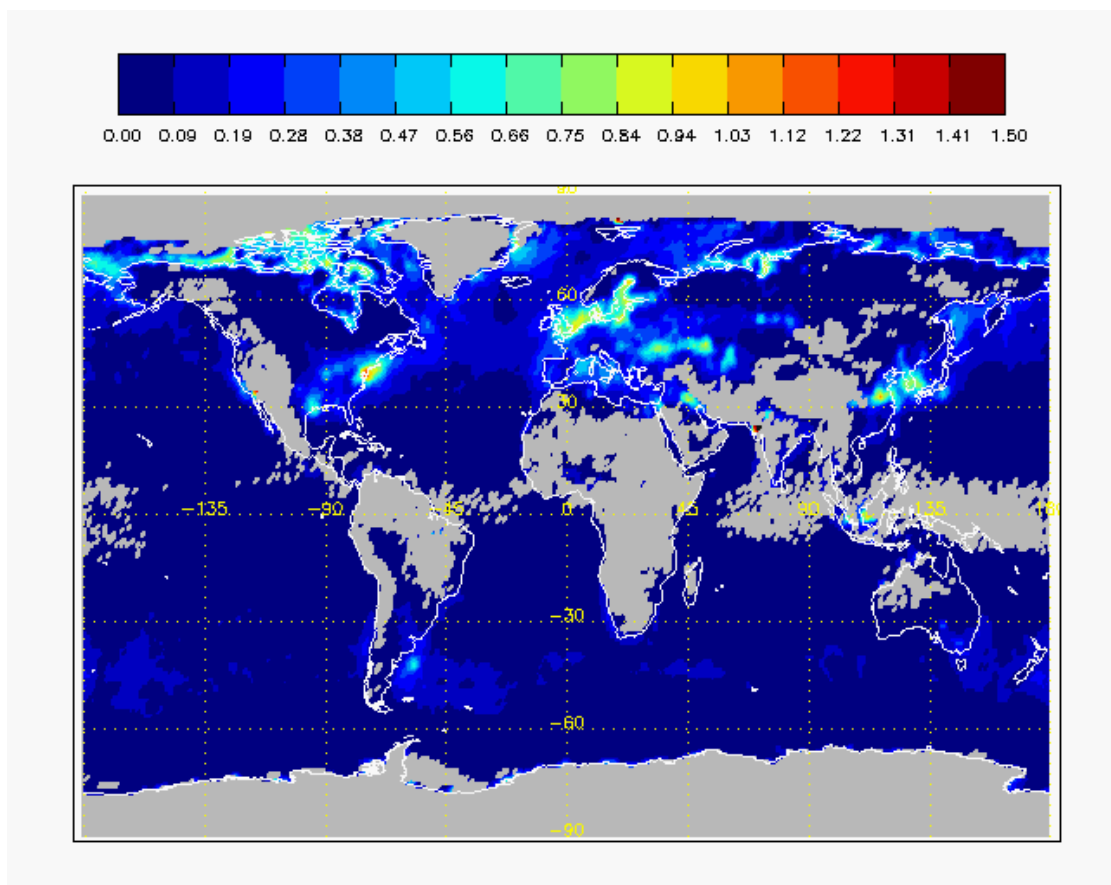


Figure R1 – Ratio between the annual mean correction (SCDbelow) for undercloud leakage and the annual mean tropospheric slant column above the cloud (SCDabove = SCDdrop - SCDbelow) at 870 hPa in the CRF 50% case.

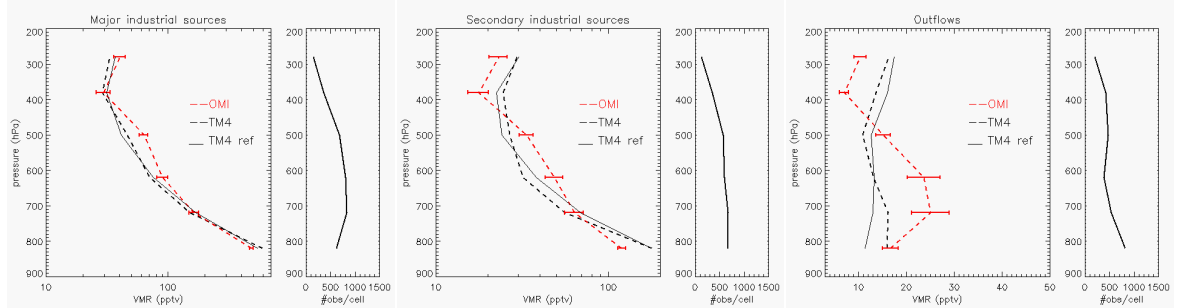
Based on this fact, the very good agreement between the cloud-slicing and model profiles, particularly in urban regions (the first row of the Fig. 8), is questionable. In polluted urban regions, the major contribution of tropospheric VCD is coming from the boundary layer (mostly below clouds) and thus NO₂ VMR is high in the boundary layer (~ppb level) and lower troposphere while very low in middle upper troposphere (<50 pptv), and the model profiles reproduce this feature well (black lines in the first row of Fig. 8). Then how can one be sure that the “good agreement” with the model in urban profiles, particularly in lower-mid free troposphere, is not coming from the $(1-\text{CRF}) * n(p_{\text{mid}})$ of the model profile instead of true free tropospheric NO₂ VMR?

Authors will need to examine the contribution of a priori information in the results, or should remove profiles that are highly affected by the a priori information.

The authors also had some reservations regarding the weight of a priori information in the

results. To clarify this matter, we did run a separate trial increasing the cloud fraction (CRF) threshold from 50% to 80%, whose main results we reproduce here:

CRF 50% - General



CRF 80% - General

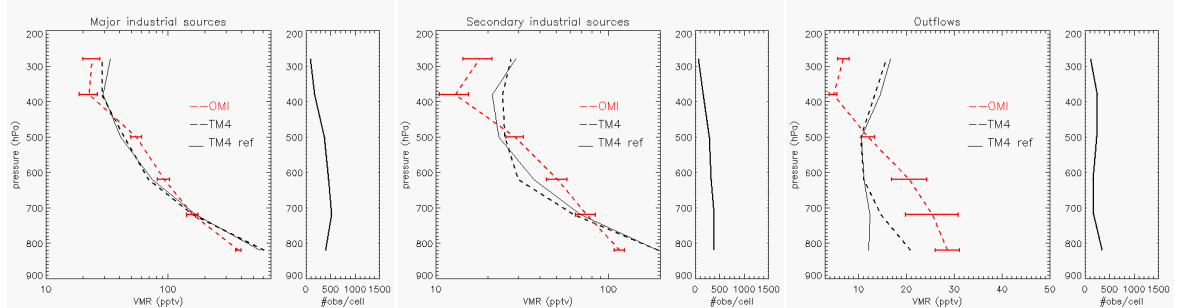
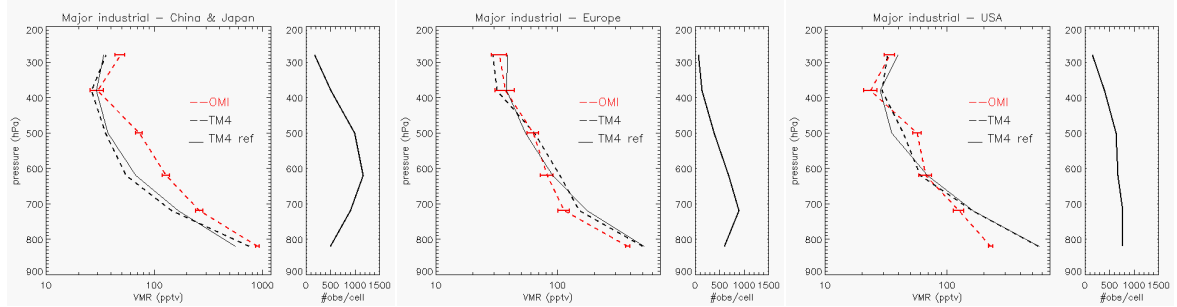


Figure R2 – Average tropospheric NO₂ profiles for the year 2006: all primary sources (left), all secondary sources (middle) and all outflows (right). Identical to Fig.9 in manuscript, but for CRF 50% case in top row, and CRF 80% case in the bottom row.

All the main features at mid-tropospheric levels persist after changing the CRF threshold from 50% to 80%. The largest change consists in a general decrease of upper tropospheric NO₂ amounts (280 & 380 hPa) in the 80% case, along with smaller biases at the lowest level (820 hPa) with decreases over polluted areas and increases over outflow areas. The overarching question is whether those differences are caused by the influence of a priori information, or by a change in representativity induced by selective sampling. The decreased NO₂ amounts at upper tropospheric levels is clearly a sampling effect, which we attribute to a poorer capture of convective activity, which has a known preference for low cloud fractions. Screening the lower cloud fractions at upper levels is screening the very source of NO₂ there (i.e. lightning events), resulting in overall lower NO₂ amounts. A critical look at the geographical distributions of NO₂ from OMI and the TM4 model at high altitudes (see Fig.5a) should persuade the reviewer of the lack of observation-to-model correlation in the 50% case. In our opinion, lowering the cloud fraction is not introducing any artificial observation-to-model agreement at upper tropospheric levels, but increasing the representativity of observations. We discuss the

matter of the lowest level separately: let us have a look over the urban regions.

CRF 50% - Major industrial sources



CRF 80% - Major industrial sources

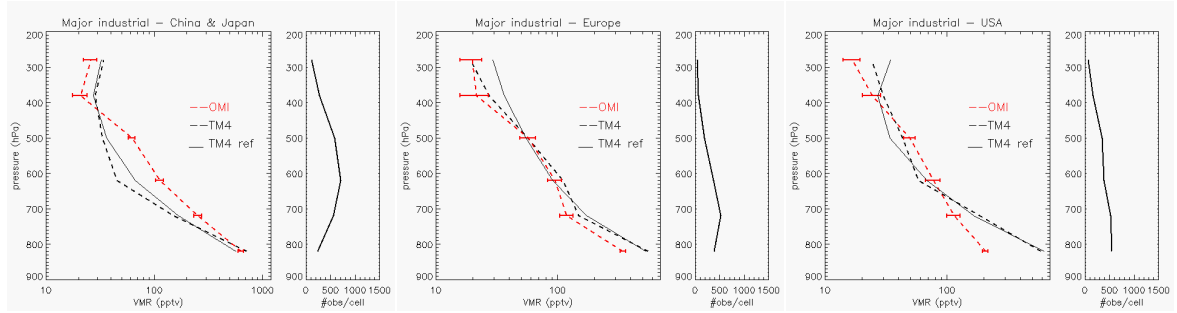
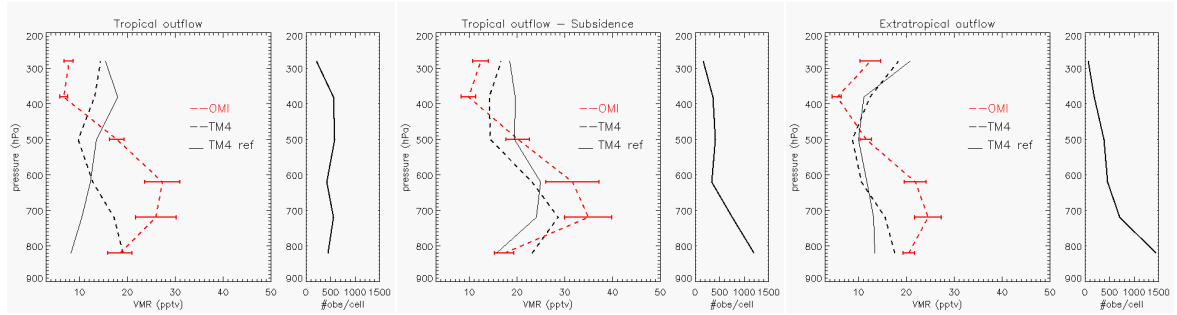


Figure R3 – Average tropospheric NO₂ profiles for the year 2006: over China (left), Europe (middle) and the USA (right). Identical to first row in Fig.8 of the manuscript, but for CRF 50% case in top row, and CRF 80% case in the bottom row.

Over industrial sources, passing from 50% to 80% CRF produces a slight decrease in lowest tropospheric NO₂ amounts, which does not seem to be consistently driven by a priori information. Changes in NO₂ at the lowest level (820 hPa) over Europe or USA are very small. Over China, the deviation from the model increases as we lower the CRF threshold – running counter to the premise of contamination by a priori information. So over urban regions, where a priori corrections would be expected to carry more influence, we do not see any clear signs of a priori information pulling results towards the reference model. Lastly, let us have a look over the outflow regions.

CRF 50% - Outflow areas



CRF 80% - Outflow areas

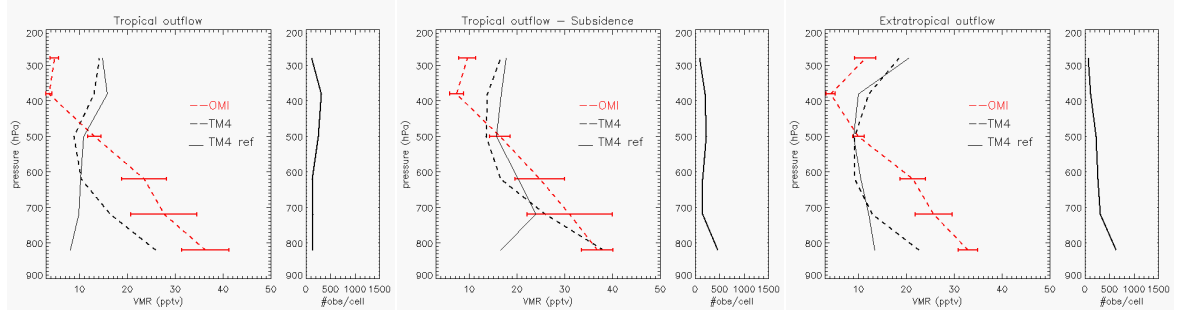


Figure R4 – Average tropospheric NO₂ profiles for the year 2006: tropical outflow (left), tropical outflows over subsidence regions (middle) and extratropical outflows (right), for CRF 50% case in top row, and CRF 80% case in the bottom row.

Over the outflow regions, passing from 50 to 80% produces a general increase of NO₂ amounts in the lowest level (820 hPa), sometimes away and sometimes towards the model. In this case, and unlike in any of the previous cases, changing the threshold is also changing the TM4 model pseudo-profiles, basically reflecting different sampling conditions (though leaving the pseudoprofile ratio basically unchanged). Note that model pseudoprofile errors (i.e. the difference between the black continuous and dashed lines in Fig.R4) at the lowest level are larger in the 80% case, which comes to say that the less samples, the less representative the result. In summary, we don't see any clear signs of a priori information contaminating the results, but we do see hints of results being influenced detrimentally by the lower sampling densities afforded by a higher CRF threshold. That is why we went for the CRF 50% threshold, which essentially means that at least 50% of the information contained in the radiance at grid level is coming from above the cloud.

Note that all the bias signatures observed in the CRF 80% case appear to be a consistent result of selective sampling: removing the lower cloud fractions induces negative biases at high altitude (when part of the lightning NO_X production is removed), negative biases at low altitude over industrial regions (when part of the advection from boundary layer NO₂ is removed) and positive biases over the outflow regions (when part of the advection from

clean boundary layer air is also removed).

The zonal mean tropospheric NO₂ cross sections for the CRF 50% and CRF 80% thresholds are appended next, to corroborate that changing the CRF threshold does not change the general picture appreciably.

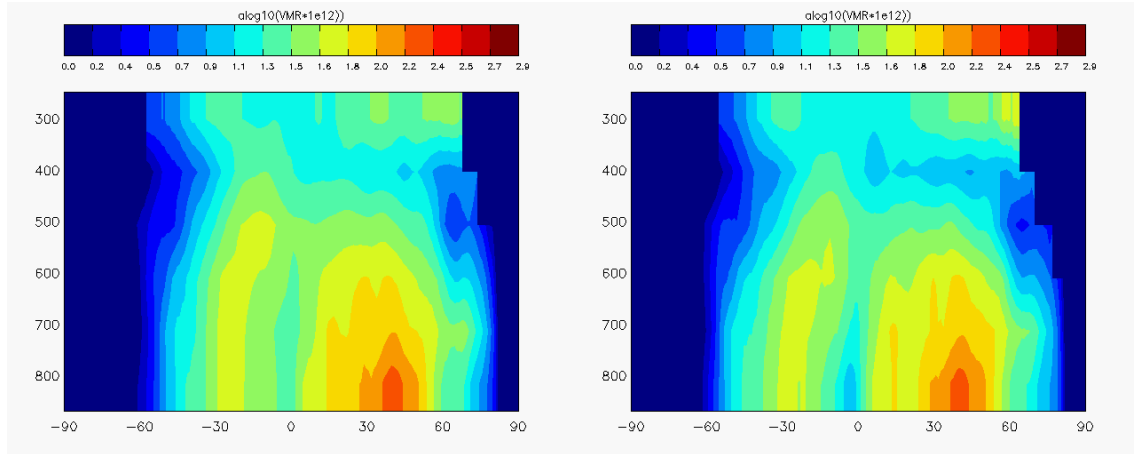


Figure R5a - CRF 50% (left) and CRF 80% (right) zonal means (as in Figure 10a of manuscript)

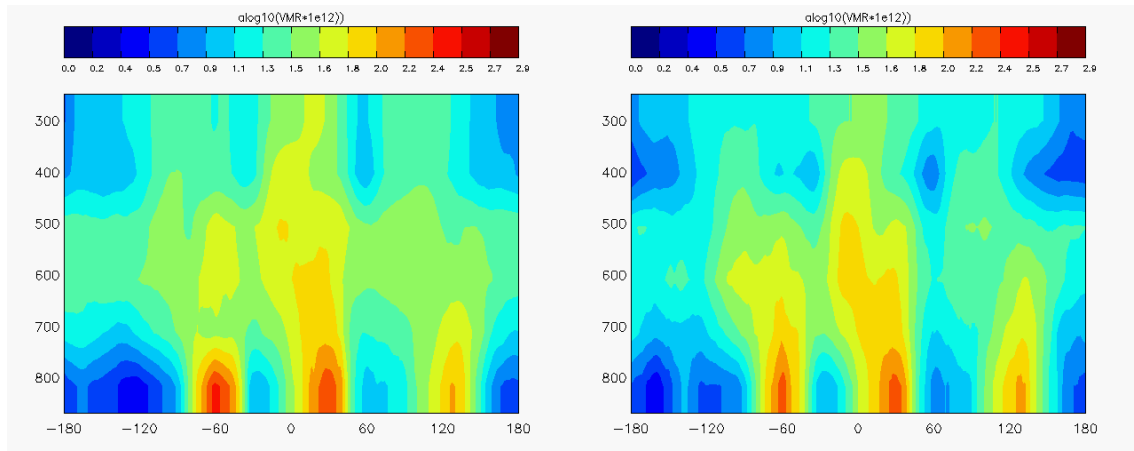


Figure R5b - CRF 50% (left) and CRF 80% (right) tropical cross-section (as in Figure 11 of manuscript)

This state of affairs was summarized in the original manuscript (first paragraph, pp 16) as:

"Results from the CRF>80% trial run include notably diminished cloud frequencies and spatial coverage, seriously thinning the population that produces the annual averages and generally damaging their representativity. This effect is particularly notable in the upper two levels (280 and 380 hPa) and to lesser extent over the large-scale subsidence area in the

lowest level, since deep convective and low marine stratocumulus clouds are not particularly extensive but have a preference for low effective cloud fractions. Excluding the contributions from these cloud types in the CRF>80% case does not change the mid-tropospheric NO₂ patterns relative to the CRF>50% case, but it is biasing the OMI aggregates in the upper troposphere low relative to the modeled average, which is not particularly sensitive to this change.”

DONE. To which we add: “The CRF>80% trial run does not show any clear signs of a priori information constraining the results, but it shows hints of results being influenced detrimentally by the lower sampling densities afforded by a higher CRF threshold.”

2) Error discussion:

p8028, l11

The “instrumental error” discussed in this subsection is actually the retrieval error. Please refer to Rodgers (JGR 1990) for proper nomenclature.

DONE. OK. Instrumental error will be referred as to retrieval error in the manuscript.

First, the retrieval error certainly is not completely random. The error analysis assumes random errors. This should be clearly stated.

DONE. OK. Retrieval errors are assumed Gaussian.

Authors “propagate” the instrumental error by assuming that the retrieval errors are random (50% for VCD and 100 hPa for cloud pressure), then compute an estimated VMR error using the summed error ratios divided by square root N (number of profiles retrieved) (Eq. 9). Please provide a reference or mathematical basis for this formulation.

Please see below.

The authors should compute standard error of the retrieved VMR, using the standard deviation of retrieved VMRs (for a grid box, per each pressure level for the desired time period) and dividing the standard deviation by the square root of N. This is the most direct way to obtain the standard error of the VMR, since the standard error of the mean is the standard deviation of the SAMPLE distribution divided by square root of the number of

profiles (given that one profile retrieval is one sampling trial).

Please note that we do not compute VMRs on daily or orbital basis (since one does not achieve the necessary cloud height diversity in 2x2 degree cells but in exceptional circumstances), but from the difference of annual mean VCDs. There is not a collection of VMRs per grid cell that we can use as “sample distribution” but one mean annual VMR computed from the pressure derivative of one mean annual VCD. The derivation of Eq.9 follows:

$$VMR = \text{factor} \cdot (VCD1 - VCD2)/(p1 - p2)$$

Where VCD1, VCD2, p1 and p2 are all mean annual quantities. The error propagation:

$$\delta VMR = \text{factor} \cdot \left(\frac{\delta(VCD1 - VCD2)}{p1 - p2} + \frac{(VCD1 - VCD2)}{(p1 - p2)^2} \delta(p1 - p2) \right)$$

$$\delta VMR = \text{factor} \cdot \left(2 \cdot \delta(VCD)/(p1 - p2) + \frac{(VCD1 - VCD2)}{(p1 - p2)^2} \cdot 2 \cdot \delta(p) \right)$$

Which is identical to Eq.(9) after taking into account that:

$$\delta(VCD_{\text{annual}}) = 0.5 \cdot VCD / \sqrt{N}$$

$$\delta(p_{\text{annual}}) = 100 \text{ hPa} / \sqrt{N}$$

That is, the standard error of the mean annual VCD is the standard error of the single VCD retrieval (assumed 50% for the OMI vertical column density, and 100 hPa for the O2-O2 cloud pressure) divided by the square root of the number of retrievals N per cell per year:

$$\delta VMR = \text{factor} \cdot \left(VCD/(p1 - p2) + \frac{(VCD1 - VCD2)}{(p1 - p2)^2} \cdot 2 \cdot 100 \text{ hPa} \right) / \sqrt{N}$$

p8038 l9: “and scaling by the square root of the number profiles collected per grid cell”

Similar to the comment on the error discussion in p8028, putting VMR errors divided by square root N (the number of profiles in a given region) may be too optimistic. As a result of the issues discussed above, the presented error bars in Fig. 8 and 9 may be unrealistically small. Since the cloud-slicing technique uses a very marginal variation of NO2 VCD depending on cloud pressure (which also has large uncertainties), the errors in the resulting VMRs should be fairly large for individual cases.

Our approach does not use single VMR or cloud pressures instances. We use the pressure derivative of the annual mean VCD along with the annual mean cloud pressure instead.

There may be more sources of systematic error (other than the pseudoprofile error), including but not limited to the error from uncertainties in a priori profiles and the stratospheric column. While cloud-slicing NO₂ profiles show very good agreement with model NO₂ profiles, the authors make a number of statements based on the differences between NO₂ profiles from cloud-slicing and TM4 model throughout Sect. 3. Error discussion is an issue in this case because some of the statements are valid only if the cloud-slicing profile errors are smaller than the difference between the profiles from cloud-slicing and the model. I suspect the errors of the cloud-slicing NO₂ VMRs are greater than the error bars presented in the paper. OMI VMR errors are correlated with model errors and this needs to be discussed. The magnitude of errors needs to be carefully examined and the discussion also needs to be revised accordingly.

DONE. The authors agree with the reviewer that error analysis is an issue. The retrieval error bars are indicative of what the instrumental/retrieval precision for single columns is relative to the resulting pseudoprofile error, suggesting that systematic errors dominate due to the sparse sampling nature of the cloud slicing technique. Other sources of systematic error may also intervene, as the reviewer points out, including uncertainties in a priori corrections and errors in the stratospheric column. The effect of uncertainties in the a priori corrections is difficult to estimate, since we take the model that performs the corrections as reference as well, lacking a better ground truth, although the CRF 80% trial run demonstrates that their effect is not appreciable (and certainly not as large as sampling related errors). The effect of errors in the OMI stratospheric column are expected to be small, since stratospheric columns only show a small additive bias (Belmonte Rivas et al., “Intercomparison of daytime stratospheric columns”, AMT, 2014) that is bound to cancel via the pressure derivative. One could also include errors from the collocation of model and OMI clouds in this category, which was also mentioned earlier in the manuscript – these errors refer to the fact that we assume that cloud altitudes and fractions in the model are identical to those observed by OMI, which is not entirely correct – but we have no means to estimate its magnitude, safe for assuming that they are small in a statistic sense. Lacking any external validation means, all we can do is describe the nature of these errors, how to bypass them when possible, and expect that the final picture afforded by observations is solid and convincing enough to motivate further studies and a global validation campaign. We do make a number of statements based on the

comparison of observations against the TM4 model, but we are aware that they remain on the level of plausible until cloud-slicing profiles are validated. All in all, section 2.1.3 on profile errors in the manuscript is revised to include these comments.

The section 2.1.3 is hard to follow in general. The section heading of Pseudoprofile errors doesn't well represent the rest of the section that includes retrieval error. The subsection Pseudoprofile (systematic) error really focuses on a correction method. This section should be reorganized and rewritten for clarity.

DONE. Agreed. Section 2.1.3 as been rewritten and reorganized as outlined above, also following commentary from Reviewer #3. The section title is changed from "Pseudoprofile errors" to "Error analysis".

3) p8027, l15

Authors collect OMI observations where cloud radiance fraction (CRF) > 20% (equivalent to cloud effective fraction > 10%), while using grid cell data with CRF > 50%. Cloud pressure errors need to be considered, because the error of cloud pressure is proportional to $1/CRF$. Cloud radiance fraction > 50% for overall measurements would be a proper threshold for cloud slicing technique.

As a pre-processing step, we use the CRF 20% threshold when collecting observations into grid cells to ensure that all bins are as densely populated as possible (thus avoiding spatial representation issues with the lower resolution model, whose cells cannot discriminate between low and high cloud fractions). Then a final CRF 50% threshold is applied at grid level (both to model and observation cells), to ensure that only those cells whose aggregated or mean CRF is above 50% are included in the analysis. Thus the final or effective CRF threshold is 50%. The aggregated or mean cloud pressure in the cell may be less accurate when including lower CRFs in the cell, but the alternative, i.e. raising the CRF threshold for observations that go into the cell appears to be biasing the sample distribution of the observation cell relative to that in the model. We found that applying an overall 50% threshold before gridding was screening many of the convective events at high altitude (which have a known preference for low cloud fractions), negatively biasing the upper tropospheric NO₂ amounts relative to the model and deteriorating the overall representativity of the observation cell. So that option was discarded.

4) p8042, l20-21: "total tropospheric NO₂ column from the cloud-slicing technique"

By nature, we can only use partial columns in cloud-slicing technique since this technique uses above-cloud columns only, i.e. from cloud pressure level to tropopause, at least for OMI NO₂ column. Then what does the “total cloudy tropospheric NO₂ column for OMI” used to produce the right panels of Fig. 13 and Fig. 14 mean?

DONE. The total tropospheric NO₂ column (VCD_{slicing}) from the cloud-slicing technique is calculated as the sum of partial vertical column densities across cloud height layers using the annual mean VMR pseudo-profiles as:

$$VCD_{slicing} (\text{lat}, \text{lon}) = \text{SUM}_{i=1, \dots, 6} \{ \text{VMR}_i (\text{lat}, \text{lon}) * (\langle p_{i+1} \rangle - \langle p_i \rangle) / C \}$$

Where C is the same constant defined in Eq.8. Absent VMR grid values (like at high altitudes over tropical subsidence regions or low over the African continent) are ignored without provision of any new a priori information. The manuscript is revised to include the expression above.

If the authors separately derived “total tropospheric OMI NO₂ column for cloudy condition” (other than the above-cloud column), they should state the method in the manuscript.

No.

In addition, if “total tropospheric NO₂ column from the cloud-slicing technique” for OMI is calculated in some way, the calculated “total cloudy tropospheric OMI column” includes a priori information instead of “true” information of tropospheric NO₂ below clouds. Then, this comparison might not be a valid consistency check.

The total tropospheric NO₂ column from cloud slicing (i.e. the total cloudy tropospheric column) is calculated as indicated above, without provision of any a priori information – other than that used to perform the undercloud leak corrections when forming the VMR pseudoprofiles.

5) p8043 l12-18

The left panel of Fig. 14 shows that the OMI NO₂ tropospheric column in clear conditions seems smaller than the model column over the northeastern US, Europe and Japan while greater over China, India, Middle East and middle Russia for the year of 2006. But it might not necessarily be caused by the NO₂ long term trend, because it can result from

uncertainties in the 2006 emission inventory or other inputs/dynamics in the model.

That is the point. The emission inventory in this CTM is prescribed by the POET database, which is typical of the years 1990-1995. So the anomaly (clear sky tropospheric OMI to TM4 in 2006) indicates that the inventory is outdated, indirectly reflecting changes that over time are consistent with known NO₂ long-term trends. Since the anomaly is most notable at the level closest to the surface over urban centers, we consider the effects of other inputs/dynamics as secondary.

Minor comments:

Overall figures: the authors need to enlarge labels and numbers in the figures so they are readable. The figure should be understandable from the caption and this is not always the case.

DONE. Captions and figure labels have been revised, one by one, for readability and clarity.

p8021, l15

The paragraphs under “OMI NO₂ columns” actually describe OMI NO₂ and OMI O₂-O₂ cloud product, so an appropriate heading is needed.

DONE The heading is changed from “OMI NO₂ columns” to “OMI NO₂ products”.

p8025, l2 and throughout the manuscript: “CTP” in the equation 3 seems to mean Cloud Top Pressure according to Fig. 2. However, as explained in p8022 l7-8, the cloud pressure retrieved from O₂-O₂ product the cloud midlevel pressure and is different from the cloud top. Therefore, it is not appropriate to call it CTP. In addition, any acronym that is used in the manuscript needs to be explained in the manuscript, not only in the figure caption, for clarity.

DONE Agreed. The term Cloud Top Pressure and its acronym CTP are changed into CLP for Cloud Level Pressure where relevant across the manuscript.

p8025, l15: “Where AMF is the total airmass factor.”

In this circumstance, AMF here seems to be total tropospheric AMF for mixed cloudy scenes, which is CRF*AMF_{cloudy} + (1-CRF)*AMF_{clear}, where AMF_{cloudy} is the AMF for a fully

cloudy scene with a given cloud pressure and AMF_{clear} is the AMF for a fully clear scene. Is this correct? It should be better stated in the manuscript.

DONE. AMF is the total airmass factor (first variable in the Temis NO₂ data field) used to compute $VCD = SCD/AMF$. It is different from the tropospheric airmass factor (fourth variable in the Temis NO₂ data field) used to compute $VCD_{trop} = (SCD - SCD_{strat})/AMF_{trop}$. The reference is in Boersma et al., "Dutch OMI NO₂ (DOMINO) data product v2.0: HE5 data file user manual". A clarifying note is inserted in the manuscript.

p8026, l17-19: "Using OMI's cloud information to sample the TM4 model amounts to assuming that the model is driven by the same cloud conditions observed by the instrument." This sentence is not clear.

DONE. The sentence is rephrased into "Using OMI's cloud information to sample the TM4 model amounts to assuming that cloud altitudes and fractions in the model are identical to those observed by OMI."

p8026, l20: "but we also know that current model cloud fields are able to reproduce the average geographical and vertical distribution of observed cloud amounts reasonably well" Authors need a proper reference for this statement.

DONE. The TM4 model uses cloud fields interpolated from the ECMWF model. An analysis of the model cloud fields from ECHAM5 (branched from an earlier version of the ECMWF general circulation model) against CALIPSO and CloudSAT data attests to our statement (see reference to [Nam et al, 2014] in the manuscript). Also, a new reference to:

Boersma, K.F., Vinken, G.C.M., and Eskes, H.J.: Representativeness errors in comparing chemistry transport and chemistry climate models with satellite UV/Vis tropospheric column retrievals, Geoscientific Model Development Discussions, in press, gmd-2015-134, 2015.

Has also been inserted, which includes an explicit comparison between OMI and TM5 cloud fields.

p8032 l9: "total VCD column"

Does this mean "total tropospheric NO₂ VCD"?

DONE. Yes. Corrected.

p8038 l2: "15"

I see only 11 items in Table 2 and Fig 7b.

DONE. The sentence is rephrased into: "for all the 11 classes (15 classes when the primary and secondary industrial regions are subdivided into China, USA, Europa subclasses) defined in Table 2 and Fig. 7b are shown next"

p8041 l7: "observation update"

I presume "observation update" means OMI NO₂ VMR cross sections, but it is not explained in the manuscript.

DONE. Agreed. In the manuscript: "Note that in order to bypass pseudoprofile errors, the observed NO₂ pseudoprofiles are scaled in this section by the model profile-to-pseudoprofile ratio as in Eq. (13)." The sentence is appended with: "... forming what is called the observation update".

Reply to Referee #3

The study "OMI tropospheric NO₂ profiles from cloud slicing: constraints on surface emissions, convective transport and lightning NO_x" by M. Belmonte Rivas et al. applies a cloud slicing technique to clouded OMI NO₂ observations in order to derive a mean NO₂ pseudoprofile. The study is well written and contains comprehensive analysis, which indicate (regional) model shortcomings for emissions, convection, advection, or lightning NO_x, which is valuable information for the scientific community.

My main concern is that the study does not at all account for seasonality, while all involved components (NO_x emissions (heating, lightning, biomass burning), NO_x life-time, convection patterns, NO_x profiles, and cloud characteristics) can vary strongly over the year. The value of an annual mean pseudoprofile is thus questionable, as the different cloud pressure levels and the corresponding NO₂ columns are not at all equally distributed over the year.

Previous cloud slicing studies have considered seasonality (e.g. Liu et al. for CO and Choi et al. for NO₂), and I see no reason why this study does not. Thus, I recommend to perform the cloud slicing on a seasonal basis. If statistics is too low for 3 months, the seasons from several years can be merged. This requires major revisions, but will yield better interpretable pseudoprofile and very likely strengthen the discussion of the model comparison.

May this manuscript serve as a proof-of-concept regarding the amount of information that may be extracted from otherwise discarded cloudy OMI (GOME or SCIAMACHY) data. The authors are already intent on applying the cloud slicing methodology on OMI data on a seasonal (and also interannual) basis. But due to the already excessive length of this manuscript, we would prefer to leave this material for a future paper. The object of this manuscript is to describe our methodology, its shortcomings, and what potential applications it may serve. We are aware that any statements regarding the comparison with the model remain at the level of plausible at this stage, in the hopes that the picture afforded is solid and convincing enough to motivate further studies and perhaps a global validation campaign.

Further comments:

8022/7: Here, OMI "cloud pressure" is introduced and related to the cloud midlevel. Later (Fig. 2, section 3.1), the terms "cloud top pressure" and "cloud top" are used. Please use consistent terms.

DONE. Agreed. The term Cloud Top Pressure and its acronym CTP are changed into CLP for Cloud Level Pressure where relevant across the manuscript.

8023/19: VMR is not a concentration.

DONE. Agreed. The terms volume mixing ratio and concentration are used interchangeably thorough the manuscript, though here for correctness the term volume mixing ratio will be used.

8023/24: What is the lesson learned from the trial runs? How far are the results depending on the chosen pressure grid? What are the reasons for choosing exactly this grid?

In general terms, profiles do not depend on the chosen pressure grid, though their appearance (particularly their vertical resolution) does. Initially, we started with three strata defined between the surface, 720 hPa, 500 hPa and the tropopause level as being representative of low, mid-level and high level clouds. At a later stage, each strata was further subdivided into two sublevels (distributing the number of samples per strata as uniformly as possible), as we noticed that the resulting amount of samples per strata was sufficiently large to provide new profiles with a smoother and realistic appearance.

8024/16-19: Clarify that VCD_above is the *tropospheric* column above cloud

DONE. OK.

8025/19: Units are missing.

The temperature correction T_{corr} is unitless.

8028/1: Before discussing the Pseudoprofile errors, please first introduce the term Pseudoprofile in a dedicated subsection.

DONE. Agreed. The section 2.1.3 has been rewritten and reorganized, also on request of Reviewer #2.

8028/10: model true -> model ("true")

DONE. Agreed.

8029/4: It is stated that the cloud modifies the profile, but how (and how strong) is not discussed. This aspect should be extended when introducing the Pseudoprofile.

DONE. Agreed. The following text is inserted in Section 2.1.3: "There are a number of ways in which the presence of cloud may modify the underlying profile: either directly, via lightning NOx production in the upper levels, or advection of (clean/polluted) air from the boundary layer at the lower levels, or more indirectly via suppression of biomass burning at the surface or decreased photolysis under the cloud. One can appreciate that the effect

of cloud presence on the profile varies with cloud altitude, which is unfortunate, because we use changes in cloud altitude to sample the underlying profile. This state of affairs introduces a source of systematic error between the cloud-slicing estimate of trace gas concentration (i.e. the pseudoprofile) and the actual underlying profile, which we term pseudo-profile error.”

8030/18: Why is this comparison not shown? This figure might be provided as supplement.

DONE. Agreed. The annual mean NO₂ VCDs above cloud from the TM4 model (the model counterpart to Figure 3) have been inserted in the manuscript as Figure 7b.

8036/25:

we have drawn ... classes defined according ...
-> we have defined ... classes according ...

DONE. Agreed.

8043/19: actualize -> update; please provide reference(s).

DONE. Agreed. Two new references have been introduced:

Mijling, B., and R. J. van der A (2012). Using daily satellite observations to estimate emissions of short-lived air pollutants on a mesoscopic scale, *J. Geophys. Res.*, 117, D17302, doi:10.1029/2012JD017817.

Ding, J., R.J. van der A, B. Mijling, P.F. Levelt, and N. Hao (2015). NO_x emission estimates during the 2014 Youth Olympic Games in Nanjing. *Atmos. Chem. Phys. Discuss.*, 15, 6337-6372, doi:10.5194/acpd-15-6337-2015

Fig. 5: Are there also negative VMR (over ocean)? If so, please mention & shortly discuss them.

DONE. Yes, there are some instances of negative VMRs but mainly related to column differences between poorly populated cells (i.e. at high latitudes, near the tropics at low altitudes, or around the subsidence regions). These instances are identified and dealt with

by recourse to information from nearby cells, when available, or otherwise ignored. A brief mention is inserted in Section 3.2. "NO₂ VMR pseudoprofiles".

1 **OMI tropospheric NO₂ profiles from cloud slicing:**
2 **constraints on surface emissions, convective transport and**
3 **lightning NO_x**

4

5 **M. Belmonte Rivas¹, P. Veefkind^{1,2}, H. Eskes², P. Levelt^{1,2}**

6 [1]{Technical University of Delft, Delft, The Netherlands}

7 [2]{Royal Netherlands Meteorology Institute, De Bilt, The Netherlands}

8 Correspondence to: M. Belmonte Rivas (m.belmonterivas@tudelft.nl)

9

10 **Abstract**

11 We derive a global climatology of tropospheric NO₂ profiles from OMI cloudy observations
12 for the year 2006 using the cloud slicing method on six pressure levels centered about 280,
13 380, 500, 620, 720 and 820 hPa. A comparison between OMI and the TM4 model
14 tropospheric NO₂ profiles reveals striking overall similarities, which confer great confidence
15 to the cloud-slicing approach, along with localized discrepancies that seem to probe into
16 particular model processes. Anomalies detected at the lowest levels can be traced to
17 deficiencies in the model surface emission inventory, at mid tropospheric levels to convective
18 transport and horizontal advective diffusion, and at the upper tropospheric levels to model
19 lightning NO_x production and the placement of deeply transported NO₂ plumes such as from
20 the Asian summer monsoon. The vertical information contained in the OMI cloud-sliced NO₂
21 profiles provides a global observational constraint that can be used to evaluate chemistry
22 transport models (CTMs) and guide the development of key parameterization schemes.

23 **1 Introduction**

24 Global maps of tropospheric NO₂ vertical column densities (VCDs) derived from satellite
25 UV/Vis nadir sounders such as OMI, GOME and SCIAMACHY have contributed to the
26 development of a variety of applications. Clear sky observations of tropospheric NO₂ VCDs,
27 those with cloud fractions typically below 25%, have been used to constrain surface NO_x
28 emission inventories (Martin et al., 2003) (Mijling and Van der A, 2012) (Miyazaki et al.,

1 2012), detect and monitor point source emission trends (Richter et al., 2005) (Van der A et al.,
2 2008) and constrain surface NO₂ lifetimes (Beirle et al., 2011) to cite a few examples. Still
3 cloudy conditions predominate, which prevent the detection of NO₂ concentrations at the
4 surface. For OMI, more than 70% of the measurements collected in the extratropics is
5 affected by clouds and typically discarded, with the consequent loss of information. The
6 utilization of cloudy data from satellite IR and UV/Vis nadir sounders provides access to a
7 large repository of observations with potential to reveal information about trace gas
8 concentrations at different altitudes and to constrain the parameterizations of a number of
9 cloud related processes.

10 Clouds are introduced in general circulation models (GCMs) because of their broadband
11 radiative effects and direct relation with the water vapour feedbacks and precipitation (Jakob,
12 2003). Clouds also affect the redistribution of trace gases via convection and interaction with
13 chemistry, which are essential elements in chemistry transport models (CTMs). Convective
14 transport of polluted plumes (including NO_x, but also HO_x, CO and non-methane
15 hydrocarbons NMHC) from the boundary layer can cause substantial enhancement of upper
16 tropospheric ozone, an important anthropogenic greenhouse gas (Pickering et al., 1992). At
17 high altitudes, enhanced chemical lifetimes and stronger winds are also responsible for the
18 long-range transport of pollutants. Still the exchange between environment and cloud air that
19 determines the way that convective columns evolve (i.e. the entrainment and detrainment
20 rates in mass flux schemes) remains uncertain. The presence of convective clouds not only
21 transports pollutants vertically, it also removes soluble species (like HNO₃) by precipitation,
22 and modulates photolysis rates by altering the actinic fluxes above and below the cloud (Tie
23 et al., JGR, 2003). Associated with the deepest convective clouds, the production of NO_x by
24 lightning is a key component of the NO₂ budget in the upper troposphere, not only because of
25 its relation with O₃ production, but because it affects the general oxidizing capacity of the
26 atmosphere and the lifetimes of tracers destroyed by reactions with OH - like CO, SO₂ and
27 CH₄. Yet the source strength and spatial distribution of lightning NO_x emissions remain
28 uncertain – with a global best estimate of 5±3 Tg a⁻¹ (Schumann and Huntrieser, 2007).

29 In large scale global CTMs, convection and other cloud related processes such as scavenging
30 and lightning NO_x production are represented by sub-grid parameterizations. Most convective
31 parameterizations are tested against temperature and humidity profiles from radiosondes
32 (Folkins et al., 2006), but chemical tracers provide additional constraints. A number of studies

1 have tried to quantify the effect of different convective schemes on tropospheric CO and O₃
2 profiles using satellite based climatologies for comparison with model data (Mahowald et al.,
3 1995) (Barret et al., 2010) (Hoyle et al., 2011) finding the largest discrepancies in the tropical
4 middle and upper troposphere. Even though NO₂ may appear unsuitable as a tracer of air
5 motion because of its high reactivity with other NO_y members (such as N₂O₅, HNO₃, PAN,
6 NO₃⁻ and HNO₄) and the presence of time-varying sources (mainly surface emissions and
7 lightning NO_x, but also aircraft and stratospheric inflows), its short lifetime makes it attractive
8 to study very fast transport mechanisms like convection. A number of studies have
9 demonstrated the capabilities of satellite UV/Vis sounders to estimate the source strength and
10 3D distribution of lightning NO_x over cloudy scenes [(Boersma et al, 2005), (Beirle et al,
11 2006), (Martin et al. 2007) and (Miyazaki et al., 2014)]. These studies have found good
12 agreement between modeled and observed lightning NO₂ over the tropical continents – albeit
13 with discrepancies in the geographical and vertical distributions. Other studies have compared
14 the performance of lightning parameterizations against satellite lightning flash densities, like
15 (Tost et al., 2007) and (Murray et al., 2012), to conclude that it is difficult to find a good
16 combination of convective and lightning scheme that accurately reproduces the observed
17 lightning distributions - leaving the problem of the NO_x yield per flash aside. So there is a
18 clear need for measurements with which the development of model parameterizations of
19 convective transport and lightning NO_x schemes can be guided.

20 In this paper, we use a variation of the cloud slicing technique first developed by (Ziemke et
21 al., 2001) for tropospheric ozone, and later exploited by (Liu et al., 2014) for tropospheric CO
22 and (Choi et al., 2014) for tropospheric NO₂, based on the increments of gas vertical column
23 density above cloud as a function of cloud pressure within a certain longitude/latitude/time
24 cell. Obviously, large cloud fractions and some degree of cloud height diversity within the
25 cell are conditions required for this technique to produce useful results. The cloud slicing
26 approach applied by (Choi et al., 2014) on OMI NO₂ data was able to find signatures of
27 uplifted anthropogenic and lightning NO₂ in their global free-tropospheric NO₂
28 concentrations, as well as in a number of tropospheric NO₂ profiles over selected regions. In
29 this work, global annual NO₂ VMR profiles are generated at a spatial resolution of 2°x2° on
30 pressure levels centered about 280, 380, 500, 620, 720 and 820 hPa. We give particular
31 consideration to the scattering sensitivity of the OMI measurements above the cloud, as well
32 as to the representativity of the cloud-sliced profiles with regard to a cloudy atmosphere. We

1 report on results from this methodology as well as its direct applicability as observational
2 constraint using a state-of-the art chemical transport model.

3 **2 Methodology**

4 The methodology to produce observed and modeled annual climatologies of tropospheric NO₂
5 VMR profiles under cloudy scenes starts with a description of the OMI and TM4 datasets
6 involved. We introduce the pre-processing steps required to estimate NO₂ VCDs above cloud
7 from OMI slant column measurements, followed by the upscaling steps required to bring the
8 spatial resolution of the satellite observations in line with the TM4 model grid for
9 comparison.

10 ***OMI NO₂ products***

11 The NO₂ slant columns used in this work are retrieved by the UV/Vis spectrometer OMI
12 [Ozone Monitoring Instrument, (Levelt et al., 2006)] according to the KNMI DOMINO
13 version 2.0 (Boersma et al., 2007) (Boersma et al., 2011). The data files, which include total
14 and stratospheric slant columns, averaging kernel information, cloud fraction, cloud pressure
15 and assimilated trace gas profiles from the TM4 model, are available at
16 <http://www.temis.nl/airpollution/no2.html>.

17 Of particular importance to this study are the cloud pressures and fractions retrieved by the
18 OMI O₂-O₂ cloud algorithm (Acarreta et al, 2004). The OMI O₂-O₂ cloud algorithm uses an
19 optically thick lambertian cloud model with a fixed albedo of 0.8; the fraction of this
20 lambertian cloud model covering the pixel is called effective cloud fraction [$c_{\text{eff}} = (R_{\text{obs}} -$
21 $R_{\text{clear}})/(R_{\text{cloudy}} - R_{\text{clear}})$], where R_{cloudy} and R_{clear} are modeled clear and cloudy sky reflectances,
22 and R_{obs} is the observed continuum reflectance – i.e. the reflectance with the O₂-O₂ absorption
23 line removed], which is not the same as the geometric cloud fraction but an equivalent amount
24 that yields the same *top of atmosphere (TOA)* reflectance as observations; the altitude level of
25 the lambertian cloud model is then adjusted so that it results in the same amount of O₂-O₂
26 absorption as in observations [Stammes et al., 2008]. The OMI O₂-O₂ cloud pressure refers to
27 the optical radiative cloud pressure near the midlevel of the cloud and below the MODIS
28 infrared-based cloud top, which is about 250 hPa higher than OMI for deep convective clouds
29 or about 50-70 hPa higher for extratropical midlevel clouds. The OMI O₂-O₂ cloud pressure
30 has been validated against PARASOL with a mean difference below 50 hPa and a standard
31 deviation below 100 hPa (Stammes et al., 2008). The OMI O₂-O₂ cloud fraction has been
32 validated against MODIS with a mean difference of 0.01 and standard deviation of 0.12 over

Maria Belmonte Rivas 9/1/2015 10:34 AM

Deleted: *columns*

1 cloudy scenes (effective cloud fractions larger than 50% without surface snow or ice) (Sneep
2 et al., 2008). In this paper, we use the cloud radiance fraction defined as $CRF = c_{\text{eff}} R_{\text{cloudy}}/R_{\text{obs}}$
3 – which represents the weight of the air mass factor of the cloudy part.

4 *TM4 model*

5 The TM4 chemistry transport model has a spatial resolution of $2^{\circ} \times 3^{\circ}$ with 35 sigma pressure
6 levels up to 0.38 hPa (and approximately 15 levels in the troposphere) driven by temperature
7 and winds from ECMWF reanalyses and assimilated OMI stratospheric NO_2 information
8 from previous orbits. The tropospheric chemistry scheme is based on (Houweling et al., 1998)
9 using the POET emissions (Olivier et al., 2003) database based on the EDGAR inventory for
10 anthropogenic sources, which are typical of years 1990-1995, with biomass emissions of NO_x
11 based on ATSR fire counts over 1997-2003 and released in the lowest model layers. The
12 photolysis rates are calculated as in (Landgraf and Crutzen, 1998) and modified as in (Krol
13 and van Weele, 1997). In the TM4 model, the physical parameterization for convective tracer
14 transport is calculated with a mass flux scheme that accounts for shallow, mid-level and deep
15 convection (Tiedtke, 1989). Large scale advection of tracers is performed by using the slopes
16 scheme of (Russell and Lerner, 1981). The lightning NO_x production is parameterized
17 according to (Meijer et al., 2001) using a linear relationship between lightning intensity and
18 convective precipitation, with marine lightning 10 times less active than continental lightning
19 and scaled to a total annual of 5 TgN/yr (Boersma et al., 2005). The vertical lightning NO_x
20 profile for injection into the model is an approximation of the outflow profile suggested by
21 (Pickering et al., 1998). Including free-tropospheric emissions from air-traffic and lightning,
22 the total NO_x emissions for 1997 amount to 46 TgN/yr. More about this model may be found
23 in (Boersma et al., 2011) and references therein.

24 **2.1 Cloud slicing**

25 A technique initially developed for estimating upper tropospheric ozone using nadir sounders
26 (Ziemke et al., 2001), cloud slicing consists in arranging collections of trace gas VCDs
27 measured above clouds against cloud pressure over a certain area and time period in order to
28 estimate a gas volume mixing ratio (VMR) via the pressure derivative as:

29
$$VMR = 0.1 \cdot g \cdot M_{\text{air}}/N_A \cdot \frac{\partial VCD}{\partial p} \quad (1)$$

30 where $g = 9.8 \text{ m/s}^2$, $M_{\text{air}} = 28.97 \text{ g/mol}$ and $N_A = 6.022 \times 10^{23} \text{ molec/mol}$ with VCD expressed in
31 molec/cm² and cloud pressure expressed in hPa. The method determines an average trace gas

1 | volume mixing ratio over a certain area, time period and cloud pressure interval (Choi et al.,
 2 | 2014). In this paper, annual average tropospheric NO₂ VCD lat/lon grids from OMI and TM4
 3 | are produced for six tropospheric layers with bottom cloud pressures located within pressure
 4 | intervals centered at about 330, 450, 570, 670, 770 and 870 hPa. The cloud pressure intervals
 5 | used for cloud slicing were chosen after several trial runs and are laid out in Table 1 and Fig.
 6 | 1. An annual climatology of NO₂ VMR profiles is then estimated after differencing the annual
 7 | tropospheric VCD arrays above cloud with respect to pressure.

8 | Figure 1 shows the latitude-height section of annual zonal mean OMI cloud frequency for the
 9 | year 2006, showing that cloud slicing does not provide uniform global sampling. Most high
 10 | clouds (mainly deep cumulus, since cirrus pass generally undetected by OMI) occur along the
 11 | intertropical convergence zone (ITCZ) near the equator and over tropical continents, but can
 12 | also be seen in the mid-latitude storm track regions and over mid-latitude continents in the
 13 | summer; mid-level clouds are prominent in the midlatitude storm tracks, usually guided by the
 14 | tropospheric westerly jets, and some occur in the ITCZ; low clouds, including shallow
 15 | cumulus and stratiform clouds, occur essentially over the oceans but are most prevalent over
 16 | cooler subtropical oceans and in polar regions (Boucher et al., 2013). In summary, cloud
 17 | sampling proves best at low to mid altitudes in the extratropics and mid to high altitudes in
 18 | the deep tropics. On the contrary, cloud sampling is typically poor off the west coasts of
 19 | subtropical (Pacific, Atlantic and Indian) landmasses at high altitudes - which are areas of
 20 | large-scale subsidence with persistent low stratocumulus, and at low altitudes over the
 21 | tropical landmasses, particularly the Amazon basin and Central Africa.

22 | 2.1.1 NO₂ above cloud

23 | The tropospheric NO₂ vertical column density above the cloud VCD_{above} for an instrument like
 24 | OMI is defined here as a function of the total slant column SCD as:

$$25 | \quad VCD_{above} = (SCD - SCD_{strat} - SCD_{below})/AMF_{above} \quad (2)$$

26 | Where SCD_{strat} is the stratospheric slant column, SCD_{below} accounts for the slant surface
 27 | component leaked from below the cloud (i.e. the amount of surface signal that seeps through
 28 | the cloud for partially cloudy conditions), and AMF_{above} denotes the scattering sensitivity
 29 | above the cloud. The stratospheric slant column arises from TM4 model stratospheric profiles
 30 | assimilated to OMI observations over unpolluted areas (Belmonte Rivas et al., 2014). The
 31 | undercloud leaked component is defined as:

$$SCD_{below} = (1 - CRF) \cdot \sum_{ground}^{CLP} m_{clear}(p) \cdot n(p) \cdot T_{corr}(p) \quad (3)$$

Maria Belmonte Rivas 9/1/2015 11:05 AM
Deleted: T

2 Where CRF is the cloud radiance fraction, m_{clear} is the clear sky component of the scattering
3 sensitivity (purely dependent on Rayleigh scattering and surface albedo), $n(p)$ is the a priori
4 trace gas profile (i.e. the TM4 model), and T_{corr} is the OMI temperature correction defined
5 below. Note that the summation goes from the ground to the cloud level pressure CLP (see
6 Fig. 2), where the cloud level is given by the OMI O₂-O₂ cloud pressure. The scattering
7 sensitivity above the cloud AMF_{above} is defined as (see appendix A):

$$AMF_{above} = \sum_{CLP}^{tropopause} m(p) \cdot n(p) \cdot T_{corr}(p) / \sum_{CLP}^{tropopause} n(p) \quad (4)$$

Maria Belmonte Rivas 9/1/2015 10:36 AM
Deleted: top
Maria Belmonte Rivas 9/1/2015 10:36 AM
Deleted: top

8 Where m is the total scattering sensitivity [usually defined as $(1-CRF) m_{clear} + CRF m_{cloudy}$ as
9 in (Boersma et al., 2004)]. Note that the summation in this case goes from cloud level to the
10 tropopause (see Fig. 2). The total scattering sensitivity m has been derived from the averaging
11 kernel $AK(p)$ as:

$$m(p) = AK(p) \cdot AMF / T_{corr}(p) \quad (5)$$

Maria Belmonte Rivas 9/1/2015 11:08 AM
Deleted: T
Maria Belmonte Rivas 9/1/2015 11:08 AM
Deleted: T
Maria Belmonte Rivas 9/1/2015 10:37 AM
Deleted: top

12 Where AMF is the total airmass factor (used to compute the total vertical column $VCD =$
13 SCD/AMF from the total slant column SCD , and different from the tropospheric airmass
14 factor AMF_{trop} used to compute $VCD_{trop} = SCD_{trop}/AMF_{trop}$). The temperature correction is
15 defined as in (Boersma et al., 2004) and accounts for the temperature dependence of the NO₂
16 absorption cross-section and its influence on the retrieved slant column using ECMWF
17 temperatures:

$$T_{corr}(p) = (220 - 11.4) / [T(p) - 11.4] \quad (6)$$

18 The elements of the averaging kernel contain the height dependent sensitivity of the satellite
19 observation to changes in tracer concentrations and they are calculated with a version of the
20 Doubling Adding KNMI (DAK) radiative transfer model in combination with TM4 simulated
21 tropospheric NO₂ profiles. Of central importance to our cloud slicing approach is that an
22 undercloud leaked component (SCD_{below}) is removed from the tropospheric slant column, and
23 a scattering sensitivity above the cloud (AMF_{above}) is used to estimate the vertical column
24 density above the cloud VCD_{above} . This is in contrast with the methodology applied in (Choi et
25 al., 2014), where undercloud leakages are neglected (making tropospheric estimates more
26 sensitive to surface contamination, particularly at low cloud fractions), and the scattering
27 sensitivity above the cloud assumed equal to the geometric airmass factor.

1 As far as model quantities are concerned, the NO₂ column above the cloud in TM4 is simply
2 calculated as:

3
$$VCD_{above} = \sum_{CLP}^{tropopause} n(p) \quad (7)$$

Maria Belmonte Rivas 9/1/2015 11:09 AM
Deleted: *T*

4 Where $n(p)$ is the a priori trace gas profile (i.e. the TM4 model). Note that the a priori gas
5 profiles, originally reported on hybrid sigma pressure grids, have been resampled onto a
6 uniform pressure grid with steps of 23.75 hPa to simplify averaging operations. The cloud
7 level pressure that defines the model above-cloud NO₂ columns in Eq. (7) is the same OMI
8 O₂-O₂ cloud pressure used for cloud slicing. Using OMI's cloud information to sample the
9 TM4 model amounts to assuming that cloud altitudes and fractions in the model are identical
10 to those observed by OMI. We know that differences between instantaneous model and
11 observed cloud fields can be notable, but we also know that current model cloud fields are
12 able to reproduce the average geographical and vertical distribution of observed cloud
13 amounts reasonably well (Boersma et al., 2015), albeit with reports of underestimation of the
14 low cloud fractions in the marine stratocumulus regions, underestimation of the midlevel
15 cloud fractions everywhere, and slight overestimation of the high cloud fraction over the deep
16 tropics (Nam et al., 2014) - errors that are likely related to the microphysical cloud and
17 convection parameterizations. Therefore, using an observed cloud field to probe into model
18 cloud processes, though probably suboptimal in case by case studies, is likely to be fine in an
19 annual average sense.

Maria Belmonte Rivas 9/1/2015 10:57 AM
Deleted: top

Maria Belmonte Rivas 9/1/2015 11:20 AM
Deleted: the model is driven by the same cloud
conditions as observed by the instrument

20 **2.1.2 Spatial averaging**

21 A comparison of OMI observations with a model such as TM4 should also take into account
22 the inhomogeneity of the tropospheric NO₂ field, which is usually large due to the presence of
23 strong point sources and weather-scale variability. The model NO₂ columns should be viewed
24 as areal averages, given that the limit of scales represented in the model is given by its
25 resolution. Thus it is important to aggregate OMI observations to attain the same spatial
26 resolution used by the model. The OMI NO₂ VCD above cloud observations (with a nominal
27 spatial resolution of 13x24 km at the swath center) are aggregated onto daily 1°x1° longitude-
28 latitude bins – later spatially smoothed to 2°x2° – before comparison with the afternoon TM4
29 model outputs defined on a 2°x3° grid on a daily basis as in Eq. (7). The aggregated OMI
30 product collects all VCDs observed within a specified period (1 day) with solar zenith angle
31 less than 70°, surface albedo less than 30% and CRF larger than 20% at the OMI pixel level

1 (roughly equivalent to an effective cloud fraction of 10%, which is a minimum condition for
2 cloud fraction and pressure to be properly reported by OMI). No weighting is applied. At this
3 point, populating the grid bins with as many OMI measurements as possible is important in
4 order to avoid spatial representation errors between the two records (a partially filled bin may
5 not be representative of what occurs over the entire cell, which is what the model represents).
6 The aggregated CRF (and all other OMI and model quantities) are then evaluated at grid
7 resolution, and a CRF threshold of 50% at cell level is applied to both observations and model
8 data. The annual mean tropospheric VCD above cloud is then calculated per pressure layer
9 using the CLP thresholds specified in Table 1 on daily gridded OMI and TM4 NO₂ VCD
10 outputs, provided there are at least 30 measurements in a bin.

Maria Belmonte Rivas 9/1/2015 11:10 AM
Deleted: T

11 2.1.3 Error analysis

12 In the cloud slicing method, the derivation of annual mean VMR profiles from annual layered
13 VCD amounts above cloud follows as:

14
$$\langle VMR_i \rangle = C \cdot (\langle VCD_{i+1} \rangle - \langle VCD_i \rangle) / (\langle p_{i+1} \rangle - \langle p_i \rangle) \quad (8)$$

15 where C is defined as $0.1 \times g \times M_{air} / N_A$ as in Eq. (1) and the index *i* refers to the cloud level. We
16 term these objects VMR pseudoprofiles because they are constructed on the conditional
17 provision of cloud presence, and the presence of cloud modifies the underlying NO₂ profile;
18 either directly, via lightning NO_x production in the upper levels, or advection of
19 (clean/polluted) air from the boundary layer at the lower levels, or more indirectly via
20 suppression of biomass burning at the surface or decreased photolysis under the cloud. One
21 can appreciate that the effect of cloud presence on the profile varies with cloud altitude, which
22 is unfortunate, because we use changes in cloud altitude to sample the underlying profile. This
23 state of affairs introduces a source of systematic error between the cloud-slicing estimate of
24 trace gas concentration (i.e. the pseudoprofile) and the actual underlying profile, which we
25 term pseudoprofile error. One may evaluate (and further compensate for) the pseudoprofile
26 error associated to conditional cloud sampling by comparing the model VMR profile
27 estimated using the cloud-slicing technique against the underlying "true" mean NO₂ VMR
28 profile from the same model, as described below. Other sources of systematic error may also
29 intervene, including uncertainties in the a priori corrections and errors in the stratospheric
30 column. The effect of uncertainties in the a priori corrections is difficult to estimate, although
31 a separate trial run using a CRF threshold of 80% at grid level demonstrates that their effect is
32 not appreciable, and certainly not as large as conditional sampling errors. The effect of errors

Maria Belmonte Rivas 9/1/2015 11:23 AM
Deleted: Pseudoprofile errors

1 in the stratospheric column are expected to be small, since stratospheric columns only show a
 2 small additive bias (Belmonte Rivas et al., 2014) that is bound to cancel via the pressure
 3 difference. One could also include temporal representativity errors from mismatched
 4 collocations between model and OMI clouds in this category, which (Boersma et al., 2015)
 5 estimate to lie around 10%. We begin this section with a brief description of the random
 6 retrieval errors that may be derived from instrumental noise properties alone.

7

8 Retrieval (random) error

9 The retrieval error in the annual mean cloud-slicing profiles is calculated by standard error
 10 propagation of Eq. (1), assuming random Gaussian errors in the determination of single OMI
 11 observations with an uncertainty (δVCD) of 50% in the OMI vertical columns densities
 12 [Boersma, 2004], an uncertainty (δp) of 100hPa in cloud pressures (Stammes et al., 2008),
 13 and scaling by the square root of the number of OMI measurements collected per grid cell
 14 N_{grid} in a year.

$$15 \quad \delta VMR = 0.1 \cdot g \cdot \frac{M_{air}}{N_A} \cdot \left(2 \frac{\delta VCD}{\Delta p} + 2 \frac{\Delta VCD}{\Delta p} \cdot \frac{\delta p}{\Delta p} \right) \cdot \frac{1}{\sqrt{N_{grid}}} \quad (9)$$

16 *Pseudoprofile (systematic) error*

17 The extent to which cloud-slicing profiles remain physical and accurate representations of an
 18 average cloudy atmosphere is limited by the assumptions that underlie the cloud slicing
 19 difference, which goes as:

$$20 \quad VMR(p_{mid}) \propto VCD(p < p_{dn} | p_{cloud} = p_{dn}) - VCD(p < p_{up} | p_{cloud} = p_{up}) \quad (10)$$

21 In cloud-slicing, the mean VMR between the pressure levels p_{up} and p_{dn} is given by the
 22 difference between the VCD above cloud pressure p_{dn} , provided there is cloud at p_{dn} , and the
 23 VCD above cloud pressure p_{up} , provided there is cloud at p_{up} too. The problem is that the
 24 presence of cloud modifies the profile. One may think that the column difference in Eq. (10)
 25 is an approximation to what happens when clouds are located at p_{mid} , somewhere between p_{up}
 26 and p_{dn} . But assuming that the trace gas concentration profile does not change with small
 27 changes in cloud altitude (which are otherwise necessary to estimate the VMR slope) entails
 28 some error. Ideally, we would like to calculate:

$$29 \quad VMR_{true}(p_{mid}) \propto VCD(p < p_{dn} | p_{cloud} = p_{mid}) - VCD(p < p_{up} | p_{cloud} = p_{mid}) \quad (11)$$

Maria Belmonte Rivas 9/1/2015 1:32 PM

Deleted: One may evaluate the associated sampling and representation errors by comparing the model VMR profile sampled using the cloud-slicing method against the model true mean NO_2 VMR profile, as detailed below. ... [1]

Maria Belmonte Rivas 9/1/2015 3:30 PM

Deleted: instrumental

Maria Belmonte Rivas 9/1/2015 3:34 PM

Deleted: profiles

1 Now we have a unique (and physically plausible) cloud condition behind the difference,
2 $p_{cloud}=p_{mid}$, and a VMR estimate that is representative of gas concentration provided that there
3 are clouds at the p_{mid} level. Yet if we would like to obtain a VMR estimate that is
4 representative of trace gas concentration in a general cloudy atmosphere, then we would
5 calculate:

6 $VMR_{ref}(p_{mid}) \propto VCD(p < p_{dn} | \forall p_{cloud}) - VCD(p < p_{up} | \forall p_{cloud})$ (12)

7 That is, VMR_{ref} represents a mean VMR profile provided that there are clouds anywhere in the
8 column, i.e. regardless of cloud altitude. We call the difference between VMR and VMR_{true}
9 sampling error, because the cloud diversity necessary to estimate the trace gas concentration
10 is distorting the underlying profile. We call the difference between VMR_{true} and VMR_{ref}
11 representation error, because a profile measured under high cloud conditions is not
12 representative of a profile under low cloud conditions, nor in general representative of an
13 average cloudy state. The difference between the cloud-sliced VMR pseudoprofile and the
14 average profile in a cloudy atmosphere VMR_{ref} is what we call the pseudoprofile error. All
15 VMR, VMR_{true} and VMR_{ref} profiles can be calculated on account of the TM4 CTM, so that a
16 model based estimation of the sampling and representation (pseudoprofile) systematic error
17 becomes available. The general pattern of pseudoprofile errors (see Sect. 3.3) indicates that
18 biases are small in the upper three levels, largely positive (100-200%) over tropical and
19 extratropical outflows in the lower two levels, and negative (up to 100%) over the continents
20 for the lower three levels (particularly over central and South America, Australia, Canada and
21 Siberia). One way to bypass this systematic error is to scale the observed VMR
22 pseudoprofiles by the model profile-to-pseudoprofile ratio as:

23 $VMR_{ref,OMI} = VMR_{OMI} \cdot (VMR_{ref,TM4}/VMR_{TM4})$ (13)

24 This model-based pseudoprofile correction (applied in Sect. 3.4) remains subject to the
25 accuracy with which the model represents its own profiles, and should be treated with caution.

26 **3 Results and discussion**

27 **3.1 NO₂ VCD above cloud**

28 | Figure 3a shows the annual mean tropospheric NO₂ VCD aggregates on 1°x1° grids observed
29 by OMI for the year 2006 above clouds with mean pressures centered around 330, 450, 570,
30 670, 770 and 870 hPa – see Fig. 1 and Table 1. A similar set of annual mean NO₂ VCDs

1 above cloud has been extracted from the TM4 model using identical cloud sampling (i.e.
2 using the cloud fraction and cloud pressure from OMI) for comparison (see Fig. 3b).

Maria Belmonte Rivas 9/1/2015 3:44 PM
Deleted: not shown

3 Most of the lightning NO₂ emissions are expected above clouds higher than 450 hPa (i.e. the
4 upper two levels in Fig. 3a) although some deep convection may also be present over strong
5 industrial sources (like northeast US, Europe, China, and the Johannesburg area) or biomass
6 burning sources in central Africa, the Amazon basin or northeast India, complicating the
7 problem of process attribution.

8 The two middle levels in Fig. 3a are expected to carry, along with the NO₂ burden inherited
9 from the upper levels, additional signatures from frontal uplifting into the mid-troposphere by
10 conveyor belts over major industrial sources in northeast US, central Europe and China, as
11 well as convective transport of biomass burning sources over central Africa, South America,
12 Indonesia and northern Australia. The strong convective signatures of surface industrial and
13 biomass burning sources, along with their low tropospheric outflows, dominate the two lowest
14 levels in Fig. 3a. Note the extensive lack of data over the tropical continents at low altitudes, a
15 region where persistent high cloud precludes penetration into the lowest levels, and over the
16 subtropical subsidence areas.

17 By differencing the annual average VCD arrays with respect to pressure, we expect to
18 separate the contributions from different altitudes to the total tropospheric VCD column. But
19 before that, let us take a look at the scattering sensitivities above cloud and the effects of
20 correcting for undercloud leakage in these results. Fig. 4 shows the annual mean tropospheric
21 scattering sensitivity above cloud level [AMF_{above} in Eq. (4)] applied to generate the OMI
22 NO₂ VCDs shown in Fig. 3a. Globally, the tropospheric scattering sensitivity above the cloud
23 does not deviate more than a 10% from the geometric airmass factor at most cloud altitudes,
24 except at the lowest levels, where it suffers reductions of up to 30%. This reduction in
25 scattering sensitivity at the lowest cloud levels may come as a surprise, particularly when
26 clouds are known to boost the scattering sensitivity just above the cloud top. However, the
27 pronounced decrease in scattering sensitivity at the lowest cloud levels is related to
28 penetration of substantial amounts of NO₂ (from strong or elevated surface sources) into the
29 cloud mid-level, where extinction acts to reduce the scattering sensitivity. Other than the
30 extinction effect, the variability in scattering sensitivity is governed by changes in the
31 observation geometry (AMF_{above} decreases as the sun angle increases) and the temperature

1 correction introduced in Eq. (6), which is responsible for the subtropical bands and the
2 variability at high southern latitudes.

3 The corrections for the surface leaked component introduced in Eq. (3) are largest (not
4 shown) over polluted regions for the highest clouds (up to 100-200%) and smallest over clean
5 areas like the oceans. In order to verify that the model-based undercloud leak corrections do
6 not appreciably change the OMI NO₂ VCDs arrays, we have performed a separate trial run
7 where the CRF threshold (at grid level) is increased from 50% to 80% to conclude that none
8 of the prominent VCD signatures seen in Fig. 3a (or none of the VMR features that we will
9 see later) changes appreciably in the restricted CRF>80% case. Results from the CRF>80%
10 trial run include notably diminished cloud frequencies and spatial coverage, seriously thinning
11 the population that produces the annual averages and generally damaging their
12 representativity. This effect is particularly notable in the upper two levels (280 and 380 hPa)
13 and to lesser extent over the large-scale subsidence area in the lowest level, since deep
14 convective and low marine stratocumulus clouds are not particularly extensive but have a
15 preference for low effective cloud fractions. Excluding the contributions from these cloud
16 types in the CRF>80% case does not change the mid-tropospheric NO₂ patterns relative to the
17 CRF>50% case, but it is biasing the OMI aggregates in the upper troposphere low relative to
18 the modeled average, which is not particularly sensitive to this change. In summary, the
19 CRF>80% trial run does not show any clear signs of a priori information constraining the
20 results, but it provides hints of results being influenced detrimentally by the lower sampling
21 densities afforded by a higher CRF threshold.

22 3.2 NO₂ VMR pseudoprofiles

23 The annual mean tropospheric NO₂ VMR pseudoprofiles observed by OMI for the year 2006
24 are compared against their TM4 model counterparts in Figs. 5a-c. Note that pseudoprofile
25 errors do not affect this comparison, since both observed and modeled pseudoprofiles are
26 observing identical (if somewhat unphysical, because of sampling and representation issues)
27 atmospheric states. After the pressure difference, there remain some instances where negative
28 VMRs are found, but these are mainly associated to poorly populated cells (such as at high
29 latitudes, or near the tropics at low altitudes, or around subsidence regions). These instances
30 are identified and dealt with by recourse to information from nearby cells, when available, or
31 otherwise ignored.

Maria Belmonte Rivas 9/1/2015 3:49 PM
Deleted: enter

1 Many of the cloud slicing features observed at the upper two levels (280 and 380 hPa) in Fig.
2 5a can be attributed to actual biomass burning, lightning and deep convection. It may be
3 difficult to separate these components clearly without a proper seasonal analysis, although
4 one can identify areas of predominant lightning production as those regions that do not seem
5 connected via convection to surface sources underneath and use the OTD-LIS flash rate
6 climatology and the ATSR fire counts (see Fig. 6 below) as interpretation aids for attribution.
7 Positive anomalies (observations larger than modeled amounts) are detected in Fig. 5a over all
8 major industrial areas (eastern US, central Europe and eastern China) both at 280 and 380 hPa
9 levels, suggesting that deep transport of boundary layer NO₂ may be too weak in the model.
10 On the contrary, there are extensive negative anomalies (meaning observations lower than
11 modeled amounts) in background upper tropospheric NO₂ both at 280 and 380 hPa, which is
12 consistent with reports of model overestimation of the amount of NO₂ attributed to lightning
13 over the tropical oceans in (Boersma, 2005).
14 Negative anomalies in Fig. 5a are particularly large over Siberia, Amazonia and the Bengal
15 Bay. The negative anomaly over eastern Siberia, an area of predominant biomass burning,
16 could be related to excessive fire-induced NO₂ emission over boreal forests in the model
17 (Huijnen et al., 2012). In South America, lightning NO₂ contributions seen by OMI appear
18 confined mostly to the western equatorial coast (Peru, Ecuador and Colombia) on one side,
19 and southern Brasil and off the east coast of Uruguay on the other hand (more in line with the
20 OTD-LIS flash climatology shown in Fig. 6) - in stark contrast with model amounts, which
21 locate the lightning maximum further to the north over the brasiliian Matto Grosso, where the
22 maxima in precipitation related to the South American monsoon system usually takes place. It
23 is worth noting that the lightning intensity in the TM4 model is solely driven by convective
24 precipitation, although [Albrecht et al, 2011] report that convective precipitation is not always
25 well correlated with lightning in this area, showing that the most efficient storms in producing
26 lightning per rainfall are located in the south regions of Brazil. The negative anomaly over
27 Amazonia is therefore very likely related to problems with the TM4 lightning scheme. The
28 negative anomaly over the Bengal Bay, an area of maxima in precipitation related to the
29 Indian monsoon, could also be a reflection of excess model lightning linked to convection.
30 Other notable discrepancies in Fig. 5a include positive anomalies over central Africa and
31 northeast India at 280 hpa. Over central Africa, the pattern of positive anomalies bears only
32 partial resemblance with the pattern of biomass burning emission underneath (see midlevel

1 OMI VMRs in Fig. 5b) – suggesting that upper level positive anomalies in central Africa may
2 be related more to deficiencies in the lighting scheme than to convective transport. Actually,
3 (Barret et al., 2010) report that lightning flash frequencies simulated by TM4 are lower than
4 measured by the LIS climatology over the Southern Sahel, which is consistent with our
5 observations. On the other hand, the large positive anomaly observed over the Tibetan plateau
6 at 280 hPa, which significantly deviates from the OTD-LIS flash rate climatology in the area
7 (confined to the Himalayan foothills only), is likely an effect of deep transport associated with
8 the Asian monsoon. The model does show an enhancement in upper tropospheric NO₂ over
9 India, but not moving far enough north into the Tibetan plateau and failing to reproduce the
10 strong enhancements in upper tropospheric NO₂ over northeast India and Southern China
11 related to the Asian summer monsoon plume – which (Kar et al., 2004) also detected in the
12 MOPITT CO profiles.

13 The cloud slicing features observed at the mid-tropospheric levels (280 and 380 hPa) in Fig.
14 5b may be mostly attributed to mid-tropospheric convection of strong surface sources and
15 their associated outflows. We observe a remarkable agreement between model and
16 observations on the localization and intensity of major convective signals over industrial
17 sources (eastern US, central Europe, China and India) as well as over typical biomass burning
18 sources in central Africa, Indonesia and South America. Contrary to what is observed in the
19 upper levels (see prevalent negative anomalies in Fig. 5a), there are extensive positive
20 anomalies (meaning observations larger than modeled amounts) in background middle
21 tropospheric NO₂ both at 500 and 620 hPa in Fig. 5b, particularly over the tropics and
22 subtropics – which is indicative of deficient model mid-tropospheric outflows at these levels.
23 Positive anomalies over the continents are particularly large over China (with an outflow
24 related positive anomaly downwind over the Pacific), central US, and the biomass burning
25 regions in central Africa and South America. While it may be more or less clear that enhanced
26 mid-tropospheric NO₂ concentrations observed over the oceans are related to enhanced
27 convective inflows into this level (without definitely discarding a problem with NO₂ lifetime),
28 the origin of the convective anomalies remains ambiguous. A cursory look at the NO₂
29 concentrations observed at lower levels might help discriminate whether flux anomalies into
30 the mid-troposphere are related to deficiencies in model prescribed surface emissions or
31 problems with the convective transport scheme, or both.

1 For example, the pattern of anomalies over China at lowest levels (see Fig. 5c) is prominently
2 positive, but it carries a dipolar positive (China) - negative (Japan) pattern that is no longer
3 observed at higher levels. So, while it is possible that some of the mid-tropospheric
4 convective anomalies are a response to flux anomalies carried from underneath (i.e. a
5 deficiency in the originally prescribed surface emission), as it happens over eastern US and
6 Europe, where negative anomalies are carried upwards (see Fig. 5b), the overall effect does
7 not exclude net deficiencies in model convective transport. As far as biomass burning is
8 concerned, the pattern of anomalies over central Africa and South America in the lowest
9 tropospheric levels (see Fig. 5c) is unfortunately not as evident (given the lack of low cloud
10 detections) as over China but mostly neutral or slightly negative, indicating that mid-
11 tropospheric positive anomalies in this area respond to either a convective transport scheme
12 that is too weak or a model injection height that is too low.

13 The lower tropospheric levels (720 and 820 hPa) in NO₂ sampled by the cloud slicing
14 technique are shown in Fig. 5c. These levels sustain the highest NO₂ concentrations in the
15 vicinity of major industrial hubs (eastern US, central Europe and China) and the strongest
16 anomalies as well, which in this case can be linked directly to deficiencies in prescribed
17 surface emissions. All major features in the anomaly patterns at these levels can be matched
18 unambiguously to the pattern of OMI to TM4 total tropospheric NO₂ column differences for
19 clear sky-conditions shown later in Fig. 12, characterized by positive anomalies over
20 northeast US, central Europe and Japan, and negative anomalies over China. These low level
21 signatures are consistent with NO₂ increases over China, India and the Middle East, and NO₂
22 decreases over eastern US and central Europe, which are not reflected in the model emission
23 inventory. Other salient features at these levels include an interesting band of negative
24 anomalies along the ITCZ (perhaps related to rapid convective mixing of relative “clean” air
25 from the boundary layer) and extensive positive anomalies over the oceans (more so at 720
26 than at 820 hPa) – revealing deficient model outflows at high latitudes and suggesting that
27 poleward transport of NO₂ in the model may not be vigorous enough (a problem likely related
28 with horizontal diffusion in the model).

29 In summary, there is remarkable agreement between observed and modeled
30 upper/middle/lower tropospheric NO₂ amounts, their main distributions resembling each other
31 at continental scale, with localized differences suggesting that the cloud slicing technique
32 holds promise for testing model features related to anthropogenic emission, convection and

1 uplift, horizontal advection and lightning NO_x production. The major discrepancies between
2 model and observations that we infer from this study include: 1) In the upper troposphere,
3 OMI observes enhanced deep transport of NO₂ from major industrial centers relative to TM4,
4 including a prominent signal from the Asian monsoon plume over the Tibetan plateau, along
5 with a slightly different geographic distribution of lightning NO₂ (likely related to
6 shortcomings in the convectively driven model lightning scheme), combined with excess fire-
7 induced convection over Siberia and a generally weaker NO₂ background over typically clean
8 areas (which is consistent with too strong lightning emissions over the oceans). 2) In the
9 middle troposphere, OMI observes enhanced localized convective fluxes of NO₂ over
10 industrial and biomass burning areas relative to TM4, combined with extensive mid-
11 tropospheric outflows that are stronger and more widely distributed in latitude than in the
12 model. 3) In the lower troposphere, OMI observes a pattern of positive-negative anomalies in
13 NO₂ concentrations that is consistent with deficiencies in model surface emissions related to
14 known NO₂ trends.

Maria Belmonte Rivas 9/1/2015 4:11 PM
Deleted: biomass burning

15 3.3 Classification

16 In the previous section, we studied the geographical distribution of observed and modeled
17 NO₂ amounts on different pressure layers. In this section, we focus on the vertical dimension
18 by looking at NO₂ VMR amounts across pressure layers. In order to simplify the analysis, we
19 have defined a set of geographical classes based on the amount of variance contained in the
20 TM4 model NO₂ profiles. These classes characterize how much of the NO₂ content in the
21 profile can be apportioned to surface sources and how much to outflows – further subdivided
22 into outflows with low, mid or high altitude components. Annual mean NO₂ VMR profiles are
23 plotted for each class, along with reference to pseudoprofile error. A standard empirical
24 orthogonal function (EOF) decomposition of the reference TM4 profiles [VMR_{ref} in Eq. (12)]
25 is employed to characterize the geographical variance of NO₂ vertical profiles under cloudy
26 conditions and identify major spatial patterns. The first four EOF eigenvectors (out of a total
27 of six) are shown in Fig. 7a. The first EOF represents profiles with higher concentrations near
28 the surface – a profile over a surface source. The second EOF represents profiles with
29 concentrations uniformly distributed across the column – a profile for a generic outflow type.
30 The third and fourth EOF eigenvectors divide the generic outflow type into subtypes with
31 stronger high altitude (EOF3>0), low altitude (EOF3<0) or mid-tropospheric (EOF4>0)
32 components. The classes that result from applying masks based on the conditions defined in

Maria Belmonte Rivas 9/1/2015 4:12 PM
Deleted: drawn
Maria Belmonte Rivas 9/1/2015 4:14 PM
Deleted: defined according to

1 Table 2 are shown in Fig. 7b. According to the TM4 model, the classes containing all primary
2 and secondary industrial sources (i.e. strong projections on EOF1) are mainly confined to the
3 US, Europe and China. Other secondary industrial sources relate to India, the Middle East and
4 the Baykal Highway (a major road connecting Moskow to Irkutsk, passing through
5 Chelyabinsk, Omsk and Novosibirsk). Major biomass burning sources include large sectors in
6 Africa and South America, Indonesia, New Guinea, and northern Australia. NO₂ outflows
7 over the tropics (i.e. strong projections on EOF2) are subdivided into generic tropical
8 outflows (with strong upper and mid-tropospheric components, or larger projections on EOF3
9 and EOF4) and outflows over large-scale subsidence areas (with stronger lower tropospheric
10 components, or negative projections on EOF3). The extratropical outflows differ from the
11 tropical outflows in that the sign of the mid-tropospheric projection is reversed, so that
12 extratropical profiles are more C-shaped (according to the model). The boreal outflow differs
13 from the extratropical outflow in that it has an extremely large upper tropospheric component
14 (i.e. a very large projection on EOF3). Finally, we have defined a separate class, labeled clean
15 background, including all those areas without significant projections on either source or
16 outflow eigenvectors.

17 The average tropospheric NO₂ profiles estimated using the cloud slicing method on OMI and
18 TM4 datasets for all the 14 classes (15 classes when primary and secondary industrial regions
19 are subdivided geographically into China, USA and Europa subclasses) defined in Table 2
20 and Fig. 7b are shown next in Figs. 8 and 9. These plots compare the OMI and TM4 VMR
21 pseudoprofile estimates calculated in a cloud slicing fashion as in Eq. (10), along with the
22 reference TM4 VMR_{ref} profile calculated as in Eq. (12) for an average cloudy atmosphere.
23 Recall that the difference between the TM4 VMR and VMR_{ref} profiles gives an indication of
24 pseudoprofile error – or the representativity of the cloud-slicing estimate relative to a general
25 cloudy situation. The OMI VMR cloud slicing estimate is bounded by error bars calculated
26 from standard error propagation as in Eq. (9), and scaling by the square root of the number of
27 profiles collected per grid cell – also shown in right subpanels in Figs. 8 and 9.

28 The cloud-slicing estimate for the annual tropospheric NO₂ profiles over primary industrial
29 centers in eastern US, Europe and China are shown in the first row in Fig. 8. There is a
30 remarkably good correspondence between observed and modeled tropospheric NO₂ profiles
31 over these strongly emitting areas, particularly over central Europe, attesting to the accuracy
32 and representativity of the cloud-slicing estimates for yearly means. Pseudoprofile errors are

Maria Belmonte Rivas 9/1/2015 5:12 PM
Deleted: 5

1 small in these areas, so that cloud-slicing estimates remain a good representation of average
2 cloudy conditions. The OMI to TM4 VMR differences at the lowest levels are consistent with
3 known deficiencies in model prescribed surface emissions (OMI smaller than the TM4 over
4 eastern US and central Europe, but larger over China). These low level anomalies are carried
5 upwards to a level of 500-600 hPa, above which the effects of enhanced convective mid-
6 tropospheric and deep transport start to dominate regardless of the signature of the surface
7 difference. The second row in Fig. 8 show the annual tropospheric NO₂ profiles over
8 secondary industrial centers around eastern US, Europe and China. The low level features
9 related to surface emission are identical to those of the primary centers, but the signature of
10 enhanced mid-tropospheric convection is clearer - indicating that vertical transport in the
11 model is too weak or lifetime too short, regardless of the sign of the surface anomaly. The
12 sign of the OMI to TM4 difference is reversed in the upper two levels, in line with the
13 generalized model overestimation of NO₂ in the upper troposphere. The third row in Fig. 8
14 shows the cloud-slicing estimate for the annual tropospheric NO₂ profiles over secondary
15 industrial pollution centers in India, the Middle East and the Baykal Highway - note that
16 pseudoprofile errors are larger in this case. For India, the differences between OMI and TM4
17 profiles at low levels point at a large underestimation of model surface emissions, and model
18 overestimation of upper tropospheric NO₂ amounts – this upper level anomaly related to the
19 misplaced Asian summer monsoon signal, which in observations appears located over the
20 Tibetan plateau. For the Middle East, the difference between OMI and TM4 profiles points at
21 large differences at mid-tropospheric level (OMI larger than TM4). The agreement between
22 OMI and TM4 profiles for the Baykal Highway class is reasonably good – allowing for a
23 small underestimation of model surface emissions. After deep transport in China, this is the
24 class with higher upper level NO₂ amounts, most likely related to fire-induced convection
25 from boreal fires. The left panel in the fourth row in Fig. 8 shows the cloud slicing estimate
26 for the annual tropospheric NO₂ profile over tropical biomass burning regions, featuring
27 positive anomalies at middle levels and negative anomalies at lower and upper levels, again
28 pointing at defective model convective transport into the mid-troposphere (or issues with the
29 pyro-convection height). The cloud-slicing estimates for annual tropospheric NO₂ profiles
30 over typical outflow regions are shown in the middle and right panels in the fourth row
31 (tropical and tropical subsidence outflows) and left and middle panels in the fifth row
32 (extratropical and boreal outflows) in Fig. 8. As a salient feature, all of the outflow profiles
33 share a prominent mid-tropospheric plume centered around 620 hPa in the tropics and a little

1 lower in the extratropics, around 720 hPa, with NO₂ amounts much smaller than the model in
2 the upper troposphere and general agreement at the lowest level, producing profiles which are
3 generally S-shaped (instead of C-shaped as in the model). The mid-tropospheric plume is
4 likely related to enhanced convective fluxes of NO₂ over industrial and biomass burning areas
5 (but definitely not discarding issues with NO₂ lifetime or substantial chemical NO_x recycling
6 from HNO₃ and PAN sources at this level). Note also the generalized model overestimation of
7 NO₂ in the upper levels (tropical and extratropical), which is consistent with reports of excess
8 lightning NO_x production over the tropical oceans in (Boersma et al., 2005). The upper level
9 overestimation is particularly large for the boreal outflow class, which we also mentioned
10 could be related to the excess fire-induced convection over Siberia or too large NO_x emission
11 factors. Finally, the cloud-slicing estimate for the annual tropospheric NO₂ profile over the
12 clean Southern Ocean is shown on the right panel of the last row in Fig. 8, with good
13 agreement at the top levels and gradually increasing model underestimation towards the
14 surface, suggesting enhanced lateral contributions at high latitudes from horizontal eddy
15 diffusion.

16 The left panel in Fig. 9 shows the annual tropospheric NO₂ profile for all the primary surface
17 sources together (eastern US, central Europe and China), indicating that differences at surface
18 level average out globally, leaving the effects of enhanced observed mid-tropospheric
19 convection and deep transport to stand out. The signature of enhanced mid-tropospheric
20 convection becomes even clearer in the mid panel in Fig. 9, which shows the annual
21 tropospheric NO₂ profile for all secondary surface sources together (around primary sources,
22 plus India, the Middle East, the Baykal Highway and the biomass burning areas), where the
23 signature of enhanced deep transport is in this case replaced by model overestimation of upper
24 tropospheric NO₂. The model overestimation of upper level NO₂ appears clearly on the right
25 panel in Fig. 9, which shows the annual tropospheric NO₂ profile for all the outflow classes,
26 along with a prominent model underestimation of mid-tropospheric NO₂ levels. In summary,
27 and consistent with our comments on Figs. 5a-c, the average profiles that result from applying
28 the cloud slicing technique on observed OMI and modeled TM4 datasets show striking
29 overall similarities, which confer great confidence to the cloud-slicing approach, along with
30 more localized differences that probe into particular model processes and parameterization
31 schemes.

1 **3.4 Cross-sections**

2 We would like to wrap up our results in the form of observed and modeled annual zonal mean
3 and longitudinal NO₂ cross-sections along the tropics (Figs. 10a-b and 11). Note that in order
4 to bypass pseudoprofile errors, the observed NO₂ pseudoprofiles are scaled in this section by
5 the model profile-to-pseudoprofile ratio as in Eq. (13) [to form what is called the observation](#)
6 [update](#).

7 For the annual zonal mean tropospheric NO₂, the left-to-right panel comparison in Fig. 10a
8 shows that although the observation update does not change the strength of major industrial
9 emission over the northern midlatitudes at the lowest levels, the associated convective cloud
10 is reaching higher in altitude. In the tropics and southern latitudes, vertical transport of the
11 combination of biomass burning and industrial emissions is stronger and reaching higher -
12 with a prominent high plume originating from the Johannesburg area. The observation update
13 does bring notably stronger midtropospheric outflows distributed over a broader latitude band
14 and weaker NO₂ signatures at high altitude. The enhanced midtropospheric plume is best
15 appreciated in Fig. 10b, which shows the annual zonal mean tropospheric NO₂ averaged over
16 the Pacific Ocean sector (180W-135W) – the dominant sources of NO₂ over the oceans are
17 [thought](#) to include the long-range transport from continental source regions, as well as
18 chemical recycling of HNO₃ and PAN sources [Staudt et al., 2003]. [Schultz et al., 1999]
19 actually shows that the decomposition of PAN originating from biomass burning actually
20 accounts for most of the midtropospheric NO_x in the remote Southern Pacific, suggesting that
21 enhanced convective flux from surface sources may not be the only agent responsible for the
22 enhanced midtropospheric outflows observed by OMI.

23 Figure 11 shows a picture for the annual longitudinal NO₂ cross-section for tropical latitudes
24 between 10N and 20S, where the observation update raises the convective plumes from major
25 biomass burning areas in South America, central Africa and Indonesia/Northern Australia to
26 higher altitude, between 500 and 600 hPa, with a slight westward tilt and longer downstream
27 transport of cloud outflow at upper levels caused by the tropical easterly jet, and generally
28 weaker NO₂ signatures at high altitude.

29 In summary, the OMI cloud-slicing NO₂ profiles seem to suggest that raising the polluted
30 plumes to higher altitudes allows for much longer residence and chemical lifetimes, and
31 longer and more widely distributed horizontal transport of NO₂ (following poleward
32 advection and dispersion by the subtropical jet and by baroclinic waves at lower levels) in the

1 mid-troposphere. These observations are in line with reports in (Williams et al, 2010) showing
2 that the underestimation of upper tropospheric O₃ in TM4 relative to observations over Africa
3 may be linked to a too weak convective uplift using the Tiedtke scheme. The studies of (Tost
4 et al., 2007), (Barret et al., 2010) and (Hoyle et al., 2011) corroborate this finding, indicating
5 that the vertical extent of tropical convection and associated transport of CO and O₃ in the
6 middle and upper troposphere is underestimated in Tiedtke based models. Accurately
7 constraining the convective transport in CTMs should contribute to the determination of the
8 vertical distribution of lightning NO_x, since knowledge of the extent of mixing of air into the
9 cloud as a function of altitude is required to separate the NO_x produced by lightning from that
10 produced by upward transport (Dickerson, 1984).

11 **3.5 Consistency check**

12 Because of their annual and global character, we do not have any direct means to validate the
13 OMI annual tropospheric NO₂ profile climatology estimates in the same way that it has been
14 done, for example, in [Choi et al., 2014]. But we can check their consistency by demanding
15 that the total tropospheric NO₂ column from the cloud-slicing technique does not deviate
16 significantly from the total tropospheric NO₂ column observed in clear sky conditions (see
17 Fig. 12). The total tropospheric NO₂ column VCD_{slicing} from the cloud slicing technique is
18 calculated as the sum of partial vertical column densities obtained from the annual mean
19 pseudoprofile VMR as:

20
$$VCD_{slicing}(lat, lon) = \sum_{i=1, \dots, 6} VMR_i(lat, lon) \cdot (\langle p_{i+1} \rangle - \langle p_i \rangle) / C \quad [14]$$

21 Where C is the same constant defined in Eq.(8). Note that absent VMR grid values (such as at
22 high altitude over subsidence regions, or at low altitude over the tropical continents) are
23 ignored without provision of a priori information.

24
25 We do know that there are some basic differences between NO₂ profiles observed under clear
26 and cloudy conditions though. In the TM4 model, the differences between cloudy
27 (CRF>50%) and clear (CRF<25%) profile climatologies (see left panel in Fig. 13 below),
28 show strong negative anomalies over the biomass burning areas (central Africa, southern
29 America, northern Australia, southern India, but also in the Persian Gulf and Turkestan) most
30 likely related to fire suppression during the wet/cloudy season. Over industrial areas (USA,
31 Europe and China) a more complex pattern of anomalies arises that likely results from the

1 competing effects of suppressed photolysis under clouds (small positive anomaly), venting by
2 passing fronts (large negative anomalies) and accumulation patterns dependent on a
3 predominant synoptic weather type [cyclonic or anticyclonic, (Pope et al., 2014)]. This pattern
4 of differences between cloudy and clear annual NO₂ profile climatologies is well reproduced
5 by OMI observations (see right panel in Fig. 13 below). The sole difference is that OMI sees
6 larger outflows at higher latitudes in the cloudy case – perhaps a deficiency of the model in
7 redistributing its horizontal flows under frontal conditions.

8 Another more direct way to perform this consistency check is to look at the differences in
9 total NO₂ columns between model (TM4) and observations (OMI) for the clear and cloudy
10 cases separately, as shown in Fig. 14. For the clear sky case (see left panel in Fig. 14) the
11 pattern of anomalies that arises is consistent with existing long-term satellite NO₂ trend
12 studies [(van der A. et al., 2008) and (Richter et al., 2005)] that report significant reductions
13 in NO₂ in Europe and eastern parts of the United States, strong increases in China, along with
14 evidence of decreasing NO₂ in Japan, increasing NO₂ in India, Middle East, and middle
15 Russia - and some spots in central United States and South Africa. The differences between
16 model and clear-sky OMI NO₂ total columns are being used to update the surface emission
17 inventories [\(Mijling & van der A, 2012\)](#) [\(Ding et al., 2015\)](#). What is comforting is that a
18 similar pattern of differences arises in the cloudy case (using the cloud-slicing TM4 and OMI
19 profiles), and with a similar amplitude, verifying that the OMI cloud slicing columns are
20 internally consistent with the clear sky OMI observations in detecting anomalies that can be
21 ultimately related to outdated model emission inventories.

22 In Figure 14, note that the model total tropospheric NO₂ columns over clean remote areas (i.e.
23 tropical and extratropical outflow regions over the oceans) in the cloudy case do not deviate
24 in general by more than 0.1xE-15 molec/cm² from observations This is a good result,
25 showing that the estimate of the stratospheric column (by data assimilation) does not produce
26 significant cloud-cover dependent biases in the tropospheric column. If we recall that the
27 observed cloud-slicing NO₂ profile over clean remote areas is S-shaped, with a much stronger
28 mid-tropospheric component and a much reduced upper tropospheric load than in the model,
29 then we can infer that there has been as much gain in the mid-tropospheric component as
30 there has been loss at high altitude, which is another form of closure.

31

Maria Belmonte Rivas 9/1/2015 4:22 PM
Deleted: actualize

1 **4 Summary and conclusions**

2 In this paper, we derive a global climatology of tropospheric NO₂ profiles from OMI cloudy
3 measurements for the year 2006 using the cloud slicing method on six pressure levels
4 centered at about 280, 380, 500, 620, 720 and 820 hPa. The cloud-slicing profiles have been
5 estimated after differencing annual tropospheric NO₂ columns above cloud with respect to
6 pressure, using mean cloud pressures located at about 330, 450, 570, 670, 770 and 870 hPa.
7 We term these objects pseudoprofiles, since the required presence of a probing cloud
8 necessarily modifies the underlying NO₂ profile. The systematic error between the cloud-
9 sliced NO₂ pseudoprofile and the average NO₂ profile in a cloudy atmosphere is called
10 pseudoprofile error, which can be evaluated (and possibly corrected) using a CTM model.

11 The total tropospheric NO₂ content in the cloud slicing profiles is consistent with the OMI
12 clear sky total tropospheric column for the same year, after making allowance for a natural
13 change in the global NO₂ distribution that occurs in passing from clear to cloudy conditions.
14 This change includes suppression of biomass burning during the wet/cloudy season,
15 suppressed NO₂ photolysis under clouds, venting by weather fronts and accumulation patterns
16 dependent on the predominant (clear or cloudy sky) synoptic weather type. The internal
17 consistency between OMI clear-sky and cloud slicing tropospheric NO₂ columns confirms the
18 capability of cloud slicing profiles to detect CTM model anomalies that can be ultimately
19 related to problems in model emission inventories, but with additional vertical information
20 that allows distinction between surface, mid-tropospheric and upper-tropospheric processes.

21 The vertical information contained in OMI tropospheric NO₂ profiles derived from the cloud
22 slicing technique provides a wealth of information that can be used to evaluate global
23 chemistry models and provide guidance in the development of sub-grid model
24 parameterizations of convective transport, fire-induced injection, horizontal advective
25 diffusion and lightning NO_x production. Overlapping processes (i.e. the effects of deep
26 convection and lightning NO_x in the upper troposphere, the effects of midtropospheric
27 convection and anomalies in surface emissions in the mid-troposphere) as well as
28 uncertainties in the chemical degradation and NO_x recycling rates currently limit the degree to
29 which discrepancies between observations and simulations can be unambiguously attributed
30 to a single process, although the availability of observational constraints definitely constitutes
31 an improvement.

Maria Belmonte Rivas 9/2/2015 3:17 PM

Deleted: and it

Maria Belmonte Rivas 9/2/2015 3:17 PM

Deleted: directly assessed

1 As an example of such an application, we have performed a comparison between cloud
2 slicing tropospheric NO₂ profiles from OMI and the TM4 model. In the upper troposphere
3 (280 and 380 hPa levels), observed NO₂ concentration anomalies reveal excessive model
4 background NO₂ amounts which are consistent with too strong model lightning emissions
5 over the oceans (and/or too long lifetimes) combined with misplaced lightning NO₂ over
6 central Africa and South America, which is indicative of limitations in the convectively
7 driven model lightning NO_x scheme of (Meijer et al., 2001). Other anomalies suggest
8 observed enhanced deep transport of NO₂ from major industrial centers relative to TM4,
9 including a prominent signal from the Asian summer monsoon plume that the model fails to
10 place accurately, and excess model fire-induced convection over Siberia.

11 In the mid troposphere (500 and 620 hPa levels), observed NO₂ concentration anomalies
12 reveal deficient model background NO₂ amounts suggestive of too small model convective
13 inflows into this level, with deficits particularly large over China, central US, and the biomass
14 burning regions in central Africa and South America, combined with extensive outflows over
15 the oceans that are stronger and more widely distributed in latitude than in the model. This is
16 consistent with independent reports of underestimation of vertical transport by convective
17 clouds in Tiedtke based models. Raising the NO₂ plumes to higher altitudes allows for much
18 longer residence and chemical lifetimes, and longer and more widely distributed horizontal
19 transport of NO₂ following poleward advection and dispersion by the subtropical jet in the
20 mid-troposphere, all of which end up producing typical outflow profiles over the oceans that
21 are generally S-shaped with a prominent mid-tropospheric plume centered around 620 hPa in
22 the tropics and around 720 hPa in the extratropics. The role that the recycled NO_x component
23 may play in the enhanced mid-tropospheric outflows observed by OMI over remote ocean
24 regions is unclear at this stage, but the cloud slicing technique shows promise to study such
25 effects.

26 In the lower troposphere (720 and 820 hPa), observed NO₂ concentration anomalies show a
27 pattern that is consistent with deficiencies in model surface emissions related to known NO₂
28 trends characterized by NO₂ increases over China, India and the Middle East, and NO₂
29 decreases over eastern US, central Europe and Japan. The lower levels also show extensive
30 positive anomalies over the oceans (particularly at 720 hPa), which are indicative of deficient
31 model outflows at low altitudes (and/or too short model lifetimes) with deficient poleward

1 diffusion of NO₂ at low to mid-tropospheric levels, and an interesting band of negative
2 anomalies along the ITCZ.

3 To date, most data assimilation experiments using OMI NO₂ observations have focused on
4 clear-sky measurements. The current results from the cloud slicing approach provide strong
5 motivation to use both clear and cloudy pixels in assimilation experiments, as in e.g.
6 (Miyazaki et al., 2014). The vertical information related to clouds is stored in the averaging
7 kernels and can be best extracted by an assimilation procedure to improve the model profile
8 shape.

9

10 **Appendix A: Gas columns above and below cloud**

11 If the tropospheric AMF_{trop} is defined as:

12 $AMF_{trop} = CRF \cdot AMF_{cloud} + (1 - CRF) \cdot AMF_{clear}$ (A1)

13 Where the clear AMF can be expressed as:

$$\begin{aligned} AMF_{clear} &= \frac{\sum_0^{tropopause} m_{clear}(z) \cdot n(z)}{\sum_0^{tropopause} n(z)} \\ &= \frac{\sum_0^{CLP} m_{clear}(z) \cdot n(z) + \sum_0^{tropopause} m_{clear}(z) \cdot n(z)}{\sum_0^{tropopause} n(z)} \\ &= \frac{\sum_0^{CLP} m_{clear}(z) \cdot n(z)}{\sum_0^{CLP} n(z)} \cdot \frac{\sum_0^{CLP} n(z)}{\sum_0^{trop} n(z)} + \frac{\sum_0^{trop} m_{clear}(z) \cdot n(z)}{\sum_0^{trop} n(z)} \cdot \frac{\sum_0^{trop} n(z)}{\sum_0^{trop} n(z)} \\ &= AMF_{clear}_{below} \cdot \frac{VCD_{below}}{VCD_{trop}} + AMF_{clear}_{above} \cdot \frac{VCD_{above}}{VCD_{trop}} \end{aligned}$$

14 (A2)

15 Where m_{clear} is the clear-sky scattering sensitivity and $n(z)$ is the model a priori trace gas
16 profile. Similarly, the cloudy AMF can be expressed as:

Maria Belmonte Rivas 9/1/2015 11:12 AM
Deleted: T
Maria Belmonte Rivas 9/1/2015 11:12 AM
Deleted: T

$$\begin{aligned}
AMF_{cloud} &= \frac{\sum_0^{tropopause} m_{cloud}(z) \cdot n(z)}{\sum_0^{tropopause} n(z)} \\
&= \frac{\sum_0^{CLP} m_{cloud}(z) \cdot n(z) + \sum_{CLP}^{tropopause} m_{cloud}(z) \cdot n(z)}{\sum_0^{tropopause} n(z)} \\
&= \frac{\sum_{CLP}^{trop} m_{cloud}(z) \cdot n(z)}{\sum_{CLP}^{trop} n(z)} \cdot \frac{\sum_0^{trop} n(z)}{\sum_0^{trop} n(z)} = AMF_{above} \cdot \frac{VCD_{above}}{VCD_{trop}}
\end{aligned}$$

1 (A3)

2 Where m_{cloudy} is the cloudy-sky scattering sensitivity. Note that by construction:

$$3 VCD_{trop} = \sum_0^{tropopause} n(z) = VCD_{above} + VCD_{below} \quad (A4)$$

4 Then the tropospheric AMF can be written, after inserting Equations (A2) and (A3) into Eq.
5 (A1), and rearranging terms relating to above and below components separately as:

$$\begin{aligned}
AMF_{trop} &= \frac{VCD_{above}}{VCD_{trop}} \left(CRF \cdot AMF_{above} + (1 - CRF) \cdot AMF_{clear} \right) + \frac{VCD_{below}}{VCD_{trop}} (1 - CRF) \\
&\quad \cdot AMF_{below} = \frac{VCD_{above}}{VCD_{trop}} AMF_{above} + \frac{VCD_{below}}{VCD_{trop}} AMF_{below}
\end{aligned}$$

6 (A5)

7 From this formulation arise definitions for AMF_{above} and AMF_{below} :

$$8 AMF_{above} \equiv \frac{\sum_{CLP}^{trop} (CRF \cdot m_{cloud}(z) + (1 - CRF) \cdot m_{clear}(z)) \cdot n(z)}{\sum_{CLP}^{trop} n(z)} \quad (A6)$$

$$9 AMF_{below} \equiv \frac{\sum_0^{CLP} (1 - CRF) \cdot m_{clear}(z) \cdot n(z)}{\sum_0^{CLP} n(z)} \quad (A7)$$

10 Now it is straightforward to write:

$$SCD_{trop} = AMF_{trop} \cdot VCD_{trop}$$

11 Which after substitution of Eq. (A5) becomes

$$SCD_{trop} = \left(\frac{VCD_{above}}{VCD_{trop}} \cdot AMF_{above} + \frac{VCD_{below}}{VCD_{trop}} \cdot AMF_{below} \right) \cdot VCD_{trop}$$

12 $= VCD_{above} \cdot AMF_{above} + VCD_{below} \cdot AMF_{below} = SCD_{above} + SCD_{below} \quad (A8)$

13 Allowing the separation of the slant components above and below the cloud as:

Maria Belmonte Rivas 9/1/2015 11:13 AM
Deleted: T
 Maria Belmonte Rivas 9/1/2015 11:13 AM
Deleted: T
 Maria Belmonte Rivas 9/1/2015 11:14 AM
Deleted: T
 Maria Belmonte Rivas 9/1/2015 11:14 AM
Deleted: T
 Maria Belmonte Rivas 9/1/2015 11:14 AM
Deleted: T

Maria Belmonte Rivas 9/1/2015 11:15 AM
Deleted: T
 Maria Belmonte Rivas 9/1/2015 11:15 AM
Deleted: T
 Maria Belmonte Rivas 9/1/2015 11:15 AM
Deleted: T
 Maria Belmonte Rivas 9/1/2015 11:15 AM
Deleted: T

1 $VCD_{above} = (SCD_{trop} - SCD_{below})/AMF_{above}$ (A9)

2 Now, in [Boersma, ACP, 2005] the above-cloud part of the NO₂ column is retrieved by
3 removing the model predicted ghost column (integrated from the ground to the cloud level
4 pressure, identical to VCD_{below}) that is implicitly added via the tropospheric airmass factor as:

5 $VCD_{above} = SCD_{trop}/AMF_{trop} - CRF \cdot VCD_{below}$ (A10)

6 However, by virtue of Eq. (A4), formulation in Eq. (A10) in [Boersma, ACP, 2005] should be
7 changed to:

8 $VCD_{above} = SCD_{trop}/AMF_{trop} - VCD_{below}$ (A11)

9 Which is equivalent to Eq. (A9).

10

11 **Acknowledgements**

12 This work has been funded by the Netherlands Space Office (NSO) under OMI contract.

13

Maria Belmonte Rivas 9/1/2015 10:58 AM
Deleted: top

1 **References**

- 2 Acarreta, J.R., De Haan, J.F., Stammes, P.: Cloud pressure retrieval using the O₂-O₂
3 absorption band at 477 nm, *J. Geophys. Res.*, 109(D5), doi:10.1029/2003JD003915, 2004.
- 4 Albrecht, R.I., Naccarato, K.P., Pinto, O., Pinto, I.R.C.A.: Total lightning and precipitation
5 over Brazil: An overview from 12-years of TRMM satellite, *AMS Conference*, Seattle (WA),
6 January 22-27, abstract No. 185724, 2011.
- 7 Arino, O., Casadio, S., Serpe, D.: Global night-time fire season timing and fire count trends
8 using the ATSR instrument series, *Remote Sens. Environ.*, 116, 226-238, 2012.
- 9 Barret, B., Williams, J.E., Bouarar, I., Yang, X., Josse, B., Law, K., Pham, M., Flochmoen,
10 E., Liousse, C., Peauch, V.H., Carver, G.D., Pyle, J.A., Sauvage, B., Velthoven, P., Schlager,
11 H., Mari, C., Cammas, J.P.: Impact of West African Mondoон convective transport ind
12 lightning NO_x production upon the upper tropospheric composition: a multimodel study,
13 *Atmos. Chem. Phys.*, 10, 5719-5738, 2010.
- 14 Beirle, S., Boersma, F., Platt, U., Lawrence, M.G., Wagner, T.: Megacity emissions and
15 lifetimes of nitrogen oxides probed from space, *Science*, 333, 1737-1739, 2011.
- 16 Beirle, S., Spichtinger, N., Stohl, A., Cummins, K.L., Turner, T., Bocciro, D., Cooper, O.R.,
17 Wenig, M., Grzegorski, M., Platt, U., Wagner, T.: Estimating the NO_x produced by lightning
18 from GOME and NLDN data: a case study in the Gulf of Mexico, *Atmos. Chem. Phys.*, 6,
19 1075-1089, 2006.
- 20 Belmonte Rivas, M., Veefkind, P., Boersma, F., Levelt, P., Eskes, H., Gille, J.:
21 Intercomparison of daytime stratospheric NO₂ satellite retrievals and model simulations,
22 *Atmos. Meas. Tech.*, 7, 2203-2225, 2014.
- 23 Boersma, F., Eskes, H., Brinskma, E.: Error analysis for tropospheric NO₂ retrieval from
24 space, *J. Geophys. Res.*, 109, doi:10.1029/2003JD003962, 2004.
- 25 Boersma, F., Eskes, H., Meijer, E. W., Kelder, H.: Estimates of lightning NO_x production from
26 GOME satellite observations, *Atmos. Chem. Phys.*, 5, 2311-2331, 2005.
- 27 Boersma, F., Eskes, H., Veefkind, J.P., Brinksma, E.J., van der A, R.J., Sneep, M., van den
28 Oord, G., Levelt, P.F., Stammes, P., Gleason, J.F., Bucsela, E.J.: Near-real time retrieval of
29 tropospheric NO₂ from OMI, *Atmos. Chem. Phys.*, 7, 2103-2118, 2007.

- 1 Boersma, F., Eskes, H., Dirksen, R.J., van der A., R.J., Veefkind, J.P., Stammes, P., Huijnen,
2 V., Kleipool, Q.L., Sneep, M., Claas, J., Leitao, J., Richter, A., Zhou, Y., Brunner, D.: An
3 improved tropospheric NO₂ column retrieval algorithm for the ozone monitoring instrument,
4 *Atmos. Meas. Tech.*, 4, 1905-1928, 2011.
- 5 [Boersma, K. F., Vinken, G. C. M., and Eskes, H. J.: Representativeness errors in comparing](#)
6 [chemistry transport and chemistry climate models with satellite UV/Vis tropospheric column](#)
7 [retrievals, *Geosci. Model Dev. Discuss.*, in press, gmd-2015-134, 2015.](#)
- 8 Boucher, O., D. Randall, P. Artaxo, C. Bretherton, G. Feingold, P. Forster, V.-M. Kerminen,
9 Y. Kondo, H. Liao, U. Lohmann, P. Rasch, S.K. Satheesh, S. Sherwood, B. Stevens and X.Y.
10 Zhang: Clouds and Aerosols. In: Climate Change 2013: The Physical Science Basis.
11 Contribution of Working Group I to the Fifth Assessment Report of the Intergovernmental
12 Panel on Climate Change [Stocker, T.F., D. Qin, G.-K. Plattner, M. Tignor, S.K. Allen, J.
13 Boschung, A. Nauels, Y. Xia, V. Bex and P.M. Midgley (eds.)]. Cambridge University Press,
14 Cambridge, United Kingdom and New York, NY, USA, 2013.
- 15 Cecil, D.J., Buechler, D.E., Blakeslee, R.J.: Gridded lightning climatology from TRMM-LIS
16 and OTD: Dataset description, *Atmos. Res.*, 135-136, 404-414, 2014.
- 17 Choi, S., Joiner, J., Choi, Y., Duncan, B.N., Vasilkov, A., Krotkov, N., Bucsela, E.: First
18 estimates of global free-tropospheric NO₂ abundances derived using a cloud-slicing technique
19 applied to satellite observations from the Aura Ozone Monitoring Instrument (OMI), *Atmos.*
20 *Chem. Phys.*, 14, 10565-10588, 2014.
- 21 Dickerson, R.R.: Measurements of reactive nitrogen compounds in the free troposphere,
22 *Atmos. Environ.*, 18, 12, 2585-2593, 1984.
- 23 [Ding, J., van der A, R.J., Mijling, B., Levelt, P.F., and Hao, N.: NOx emission estimates](#)
24 [during the 2014 Youth Olympic Games in Nanjing, *Atmos. Chem. Phys. Discuss.*, 15, 6337-](#)
25 [6372, doi: 10.5194/acpd-15-6337-2015, 2015.](#)
- 26 Folkins, I., Bernath, P., Boone, C., Donner, L.J., Eldering, A., Lesins, G., Martin, R.V.,
27 Sinnhuber, B.M., Walker, K.: Testing convective parameterizations with tropical
28 measurements of HNO₃, CO, H₂O and O₃: Implications for the water vapor budget, *J.*
29 *Geophys. Res.*, 111, D23304, doi:10.1029/2006JD007325, 2006.

- 1 Houweling, S., Dentener, F.J., Lelieveld, J.: The impact of non-methane hydrocarbon
2 compounds on tropospheric chemistry, *J. Geophys. Res.*, 103, 10673-10696, 1998.
- 3 Hoyle, C.R., Marecal, V., Russo, M.R., Allen, G., Arteta, J., Chemel, C., Chipperfield, M.P.,
4 D'Amato, F., Dessens, O., Feng, W., Hamilton, J.F., Harris, N.R.P., Hosking, J.S., Lewis,
5 A.C., Morgenstern, O., Peter, T., Pyle, J.A., Redmann, T., Richards, N.A.D., Telford, P.J.,
6 Tian, W., Viciani, S., Volz-Thomas, A., Wild, O., Yang, X., Zeng, G.: Representation of
7 tropical deep convection in atmospheric models – Part 2: Tracer transport, *Atmos. Chem.*
8 *Phys.*, 11, 8103-8131, 2011.
- 9 Huijnen, V., Flemming, J., Kaiser, J.W., Inness, A., Leitao, J., Heil, A., Eskes, H., Schultz,
10 Benedetti, A., Dufour, G., Eremenko, M.: Hindcast experiments of tropospheric
11 composition during the summer 2010 fires over Western Russia, *Atmos. Chem. Phys.*, 12,
12 4341-4364, 2012.
- 13 Jakob, C.: An improved strategy for the evaluation of cloud parameterizations in GCMs, *Bull.*
14 *Am. Meteorol. Soc.*, doi: 10.1175/BAMS-84-10-1387, 2003.
- 15 Kar, J., Bremer, H., Drummond, J.R., Rochon, Y.J., Jones, D.B., Nichitiu, F., Zou, J., Liu, J.,
16 Gille, J., Edwards, D.P., Deeter, M., Francis, G., Ziskin, D., Warner, J.: Evidence of vertical
17 transport of carbon monoxide from MOPITT, *Geophys. Res. Lett.*, 31, L23105, doi:
18 10.1029/2004GL021128, 2004.
- 19 Krol, M.C., van Weele, M.: Implications of variations in photodissociation rates for global
20 tropospheric chemistry, *Atmos. Environ.*, 31, 1257-1273, 1997.
- 21 Landgraf, J., Crutzen, P.J.: An efficient method for online calculations of photolysis and
22 heating rates, *J. Atmos. Sci.*, 55, 863-878, 1998.
- 23 Levelt, P.F., van den Oord, G., Dobber, M.R., Malkki, A., Visser, H., de Vries, J., Stammes,
24 Lundell, J., Saari, H.: The Ozone Monitoring Instrument, *IEEE Trans. Geosci. Remote*
25 *Sens.*, 44(5), 1093-1101, 2006.
- 26 Liu, C., Beirle, S., Butler, T., Hoor, P., Frankenberg, C., Jockel, P., Penning de Vries, M.,
27 Platt, U., Pozzer, A., Lawrence, M.G., Lelieveld, J., Tost, H., Wagner, T.: Profile information
28 on CO from SCIAMACHY observations using cloud slicing and comparison with model
29 simulations, *Atm. Chem. Phys.*, 17, 1717-1732, 2014.

- 1 Mahowald, N.M., Rasch, P.J., Prinn, R.G.: Cumulus parameterization in chemical transport
2 models, *J. Geophys. Res.*, 100(D12), 26173-26189, 1995.
- 3 Martin, R.V., Jacob, D.J., Chance, K., Kurosu, T.P., Palmer, P.I., Evans, M.J.: Global
4 inventory of nitrogen oxide emissions constrained by space-based observations of NO₂
5 columns, *J. Geophys. Res.*, 108(D17), 4537, doi:10.1029/2003JD003453, 2003.
- 6 Martin, R.V., Sauvage, B., Folkins, I., Sioris, C.E, Boone, C., Bernath, P., Ziemke, J.: Space-
7 based constraints on the production of nitric oxide by lightning, *J. Geophys. Res.*,
8 112(D09309), doi: 10.1029/2006JD007831, 2007.
- 9 Meijer, E.W., Velthoven, P.F.J., Brunner, D.W., Huntrieser, H., Kelder, H.: Improvement and
10 evaluation of the parameterisation of nitrogen oxide production by lightning, *Phys. Chem.*
11 *Earth*, 26(8), 557-583, 2001.
- 12 Mijling, B., van der A, R.J.: Using daily satellite observations to estimate emissions of short
13 lived air pollutants on a mesoscopic scale, *J. Geophys. Res.*, 117(D17), doi:
14 10.1029/2012JD017817, 2012.
- 15 Miyazaki, K., Eskes, H. J., and Sudo, K.: Global NO_x emission estimates derived from an
16 assimilation of OMI tropospheric NO₂ columns, *Atmos. Chem. Phys.*, 12, 2263-2288, 2012.
- 17 Miyazaki, K., Eskes, H. J., Sudo, K., and Zhang, C.: Global lightning NO_x production
18 estimated by an assimilation of multiple satellite data sets, *Atmos. Chem. Phys.*, 14, 3277-
19 3305, 2014
- 20 Murray, L.T., Jacob, D.J., Logan, J., Hudman, R., Koshak, W.J.: Optimized regional and
21 interannual variability of lightning in a global chemical transport model constrained by LIS-
22 OTD satellite data, *J. Geophys. Res.*, 117(D20), doi: 10.1029/2012JD017934, 2012.
- 23 Nam, C., Quaas, J., Neggers, R., Siegenthaler-Le Drian, C., Isotta, F.: Evaluation of boundary
24 layer cloud parameterizations in the ECHAM5 general circulation model using CALIPSO and
25 CloudSAT satellite data, *J. Adv. Model. Earth Syst.*, 6(2), 300-314, 2014.
- 26 Olivier, J., Peters, J., Granier, C., Petron, G., Müller, J. F., and Wallens, S.: Present and future
27 emissions of atmospheric compounds, POET report #2. EU report EV K2-1999-00011, 2003.
- 28 Pickering, K.E., Thompson, A.M., Dickerson, R.R., Luke, W.T., McNamara, D.P., Free
29 tropospheric ozone production following entrainment of urban plumes into deep convection,
30 *J. Geophys. Res.*, 97, 17985-18000, 1992.

- 1 Pickering, K.E., Wang, Y., Tao, W.K., Price, C., Muller, F.: Vertical distributions of lightning
2 NO_x for use in regional and global chemical transport models, *J. Geophys. Res.*, 103(D23),
3 31203-31216, 1998.
- 4 Pope, R.J., Savage, N.H., Chipperfield, M.P., Arnold, S.R., Osborn, T.J.: The influence of
5 synoptic weather regimes on UK air quality: analysis of satellite column NO₂, *Atmos. Sci.*
6 Lett.
- 7 Richter, A., Burrows, J.P., Nuss, H., Granier, C., Niemeier, U.: Increase in tropospheric
8 nitrogen dioxide over China observed from space, *Nature*, 437, 129-132, 2005.
- 9 Russell, G.L., Lerner, J.A.: A new finite differencing scheme for the tracer transport equation,
10 *J. Appl. Meteor.*, 20, 1483-1498, 1981.
- 11 Schumann, U., Huntrieser, H.: The global lightning-induced nitrogen oxides source, *Atmos.*
12 *Chem. Phys.*, 7, 3823-3907, 2007.
- 13 Schultz, M. G., et al., On the origin of tropospheric ozone and NO_x over the tropical south
14 Pacific, *J. Geophys. Res.*, 104, 5829-5844, 1999.
- 15 Sneep, M., de Haan, J.F., Stammes, P., Wang, P., Vanbause, C., Joiner, J., Vasilkov, A.P.,
16 Levelt, P.F.: Three way comparison between OMI and PARASOL cloud pressure products, *J.*
17 *Geophys. Res.*, 113(D15), doi: 10.1029/2007JD008694, 2008.
- 18 Stammes, P., Sneep, M., de Haan, J.F., Veefkind, J.P., Wang, P., Levelt, P.F.: Effective cloud
19 fraction from the Ozone Monitoring Instrument: Theoretical framework and validation, *J.*
20 *Geophys. Res.*, 113(D16), doi: 10.1029/2007JD008820, 2008.
- 21 Staudt, A.C., Jacob, D.J., Ravetta, F., Logan, J.A., Bachiochi, D., Krishnamurti, T.N.,
22 Sandholm, S., Ridley, B., Singh, H.B., Talbot, B.: Sources and chemistry of nitrogen oxides
23 over the tropical Pacific, *J. Geophys. Res.*, 108(D2), doi: 10.1029/2002JD002139, 2003.
- 24 Tiedtke, M.: A Comprehensive Mass Flux Scheme for Cumulus Parameterization in Large-
25 Scale Models, *Mon. Weather Rev.*, 117, 1779-1800, 1989.
- 26 Tie, X., Madronich, S., Waters, S., Zhang, R., Rasch, P., Collins, W.: Effects of clouds on
27 photolysis and oxidants in the troposphere, *J. Geophys. Res.*, 108(D20), doi:
28 10.1029/2003JD003659, 2003.
- 29 Tost, H., Jockel, P., Lelieveld, J.: Lightning and convection parameterization – uncertainties
30 in global modelling, *Atmos. Chem. Phys.*, 7, 4553-4568, 2007.

- 1 Van der A, R.J., Eskes, H., Boesma, K.F., Noije, T.P.C., Roozendael, M., Smedt, I., Peters,
2 D.H.M.U., Meijer, E.W.: Trends, seasonal variability and dominant NO_x sources derived from
3 a ten year records of NO₂ measured from space, J. Geophys. Res., 113(D4), doi:
4 10.1029/2007JD009021, 2008.
- 5 Williams, J.E., Scheele, R., Velthoven, P., Bouarar, I., Law, K., Josse, B., Peuch, V.H., Yang,
6 X., Pyle, J., Thouret, V., Barret, B., Liousse, C., Houdin, F., Szopa, S., Cozic, A.: Global
7 chemistry simulations in the AMMA (African Monsoon Multidisciplinary Analysis)
8 multimodel intercomparison project, Bull. Am. Meteorol. Soc., 91, 5, 612-624, 2010.
- 9 Ziemke, J.R., Chandra, S., Barthia, P.K.: Cloud slicing: A new technique to derive upper
10 tropospheric ozone from satellite measurements, J. Geophys. Res., 106(D9), 9853-9867,
11 2001.
- 12

1

2 Table 1. Cloud pressure intervals and mean cloud pressure levels used for cloud slicing (hPa):
 3 the VCD pressure interval gives the boundaries of the cloud pressure bin. The VMR pressure
 4 interval refers to where the VMR is assumed constant after the pressure difference.

Maria Belmonte Rivas 9/1/2015 4:53 PM
Deleted: Pressure
 Maria Belmonte Rivas 9/2/2015 11:40 AM
Deleted: refers to
 Maria Belmonte Rivas 9/2/2015 11:39 AM
Deleted: where clouds may be located

	VCD Pressure Interval	<VCD pressure>	VMR Pressure Interval	<VMR pressure>
Level 1	Tropopause - 380	330	Tropopause - 330	280
Level 2	380 - 500	450	330 - 450	380
Level 3	500 - 620	570	450 - 570	500
Level 4	620 - 720	670	570 - 670	620
Level 5	720 - 820	770	670 - 770	720
Level 6	820 - 1000	870	770 - 870	820

5

6

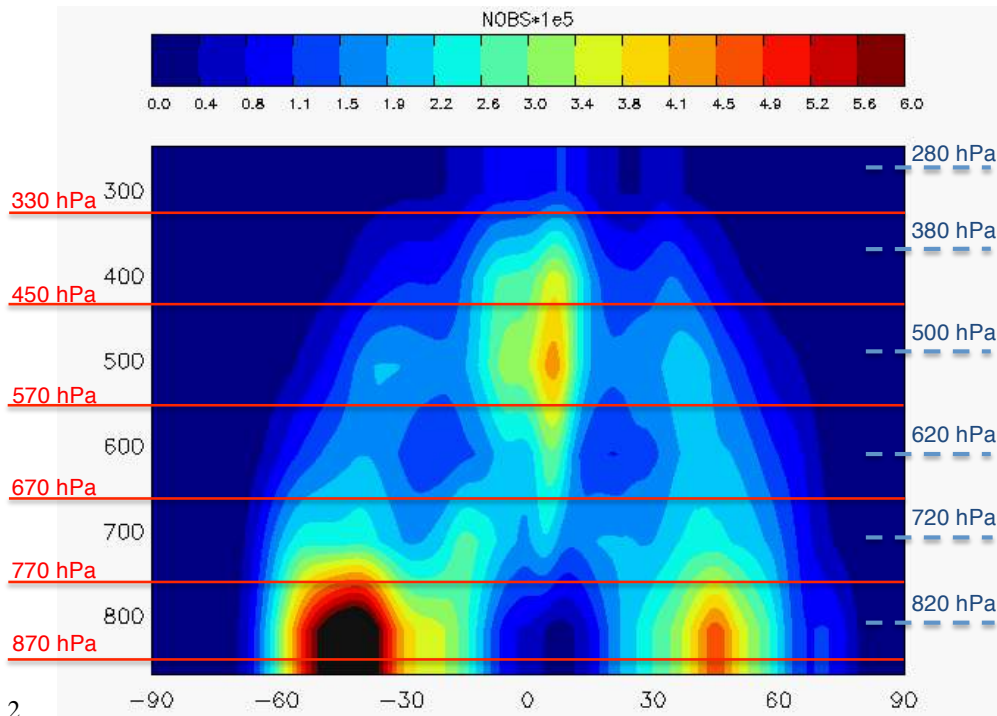
1 Table 2. Model based source and outflow class definitions based on EOF decomposition

2

Maria Belmonte Rivas 9/1/2015 6:04 PM

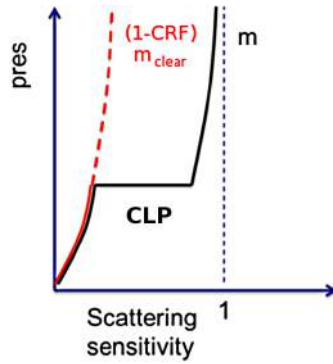
Deleted: es.

Class label	Main condition	Extra condition
Primary industrial	EOF1 > 400 pptv	US, Europe, China
Secondary industrial	100 pptv < EOF1 < 400 pptv	US, Europe, China
Biomass burning	100 pptv < EOF1 < 400 pptv	geographic
Baykal highway	100 pptv < EOF1 < 400 pptv	geographic
Indostan	100 pptv < EOF1 < 400 pptv	geographic
Middle East	100 pptv < EOF1 < 400 pptv	geographic
Tropical outflow	EOF1<50 pptv, EOF2>15 pptv	EOF3>0, EOF4>0
Tropical subsidence	EOF1<50 pptv, EOF2>15 pptv	EOF3<0
Extratropical outflow	EOF1<50 pptv, EOF2>15 pptv	EOF3>0, EOF4<0
Boreal Outflow	EOF1<50 pptv, EOF2>15 pptv	EOF3 >>0
Clean background	EOF1<15 pptv, EOF2<15 pptv	



2 | Figure 1. Latitude-height section of annual zonal mean OMI cloud frequencies (CRF>50%) -
 3 | observed during daytime around 13.45 LST. On the left in red, the bottom pressure
 4 | boundaries for the calculation of annual mean NO₂ VCDs above cloud (after Table 1). On the
 5 | right in blue, the approximate pressure for the resulting NO₂ VMR after differentiation of
 6 | VCDs (also after Table 1).
 7 |
 8 |

Maria Belmonte Rivas 9/1/2015 6:07 PM
Deleted: frequency



1

2 Figure 2. Schematic diagram of the scattering sensitivity above and below the cloud
 3 (normalized by the geometric air mass factor): CLP is the cloud level pressure, and m is the
 4 total scattering sensitivity, usually defined as $(1-CRF) m_{clear} + CRF m_{cloudy}$. The red curve
 5 illustrates a residual sensitivity to NO₂ contents below the cloud when conditions are partially
 6 cloudy.

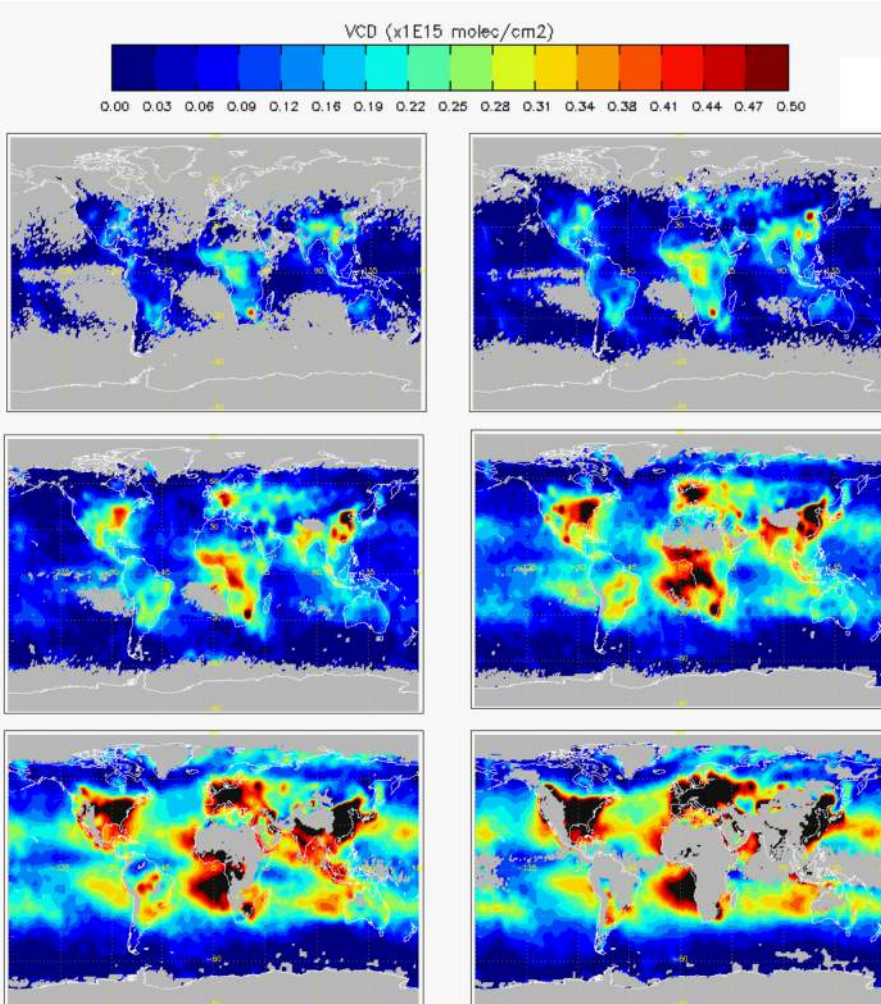
7

Maria Belmonte Rivas 9/1/2015 11:01 AM

Deleted: TP

Maria Belmonte Rivas 9/1/2015 11:01 AM

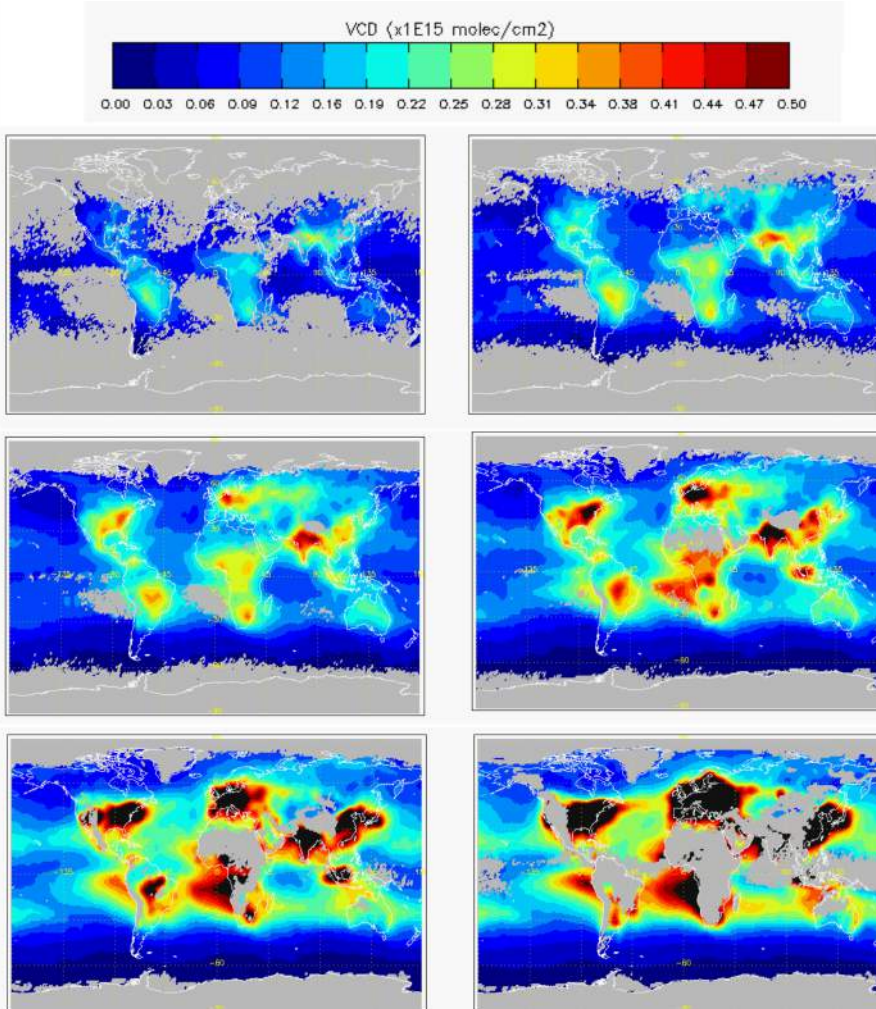
Deleted: top



1

2 Figure 3a. OMI NO₂ VCDs above cloud - average quantities for the year 2006: for high
 3 altitude clouds (top row, 330 and 450 hPa), mid altitude clouds (middle row, 570 and 670
 4 hPa) and low clouds (bottom row, 770 and 870 hPa). Grey means no data available (i.e.
 5 insufficient number of cloud detections in the cell).

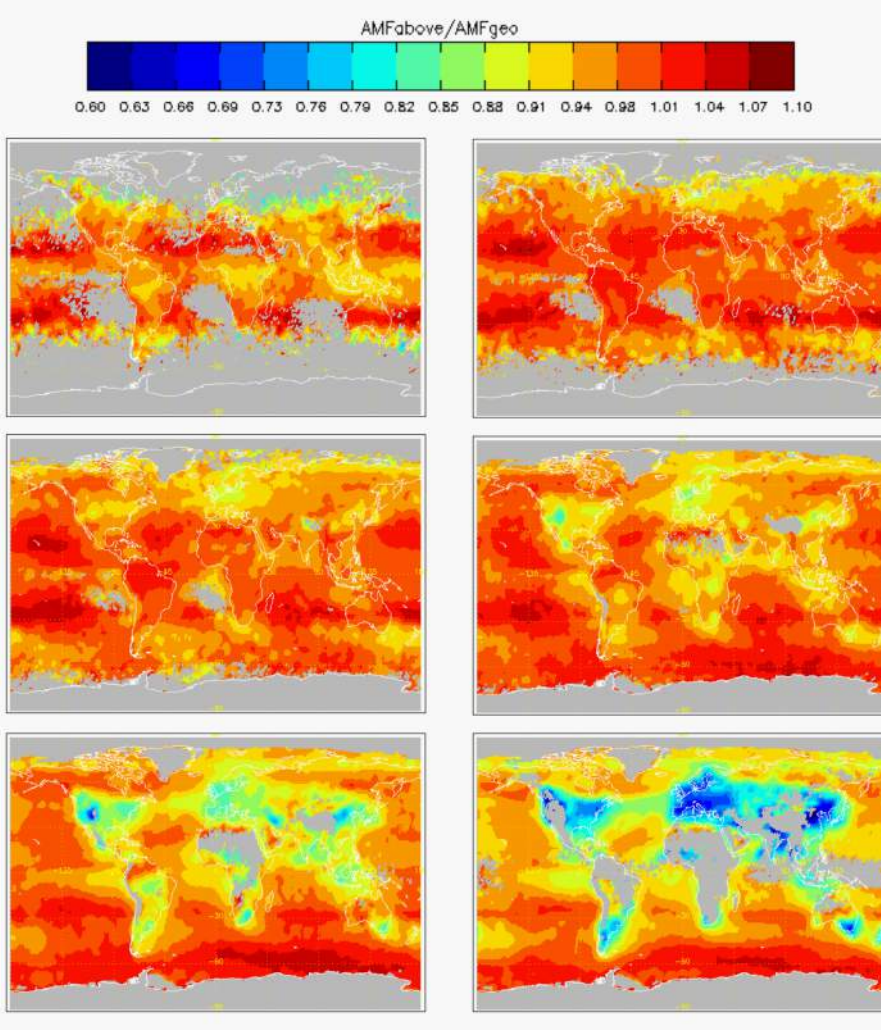
6



1

2 Figure 3b. TM4 NO₂ VCDs above cloud - average quantities for the year 2006: for high
 3 altitude clouds (top row, 330 and 450 hPa), mid altitude clouds (middle row, 570 and 670
 4 hPa) and low clouds (bottom row, 770 and 870 hPa). Grey means no data available (i.e.
 5 insufficient number of cloud detections in the cell).

6



1

2

3 Figure 4. Tropospheric scattering sensitivities above cloud level [AMF_{above}/AMF_{geo} in Eq.
4 (4)]: for high altitude clouds (top row, 330 and 450 hPa), mid altitude clouds (middle row,
5 570 and 670 hPa) and low clouds (bottom row, 770 and 870 hPa).

6

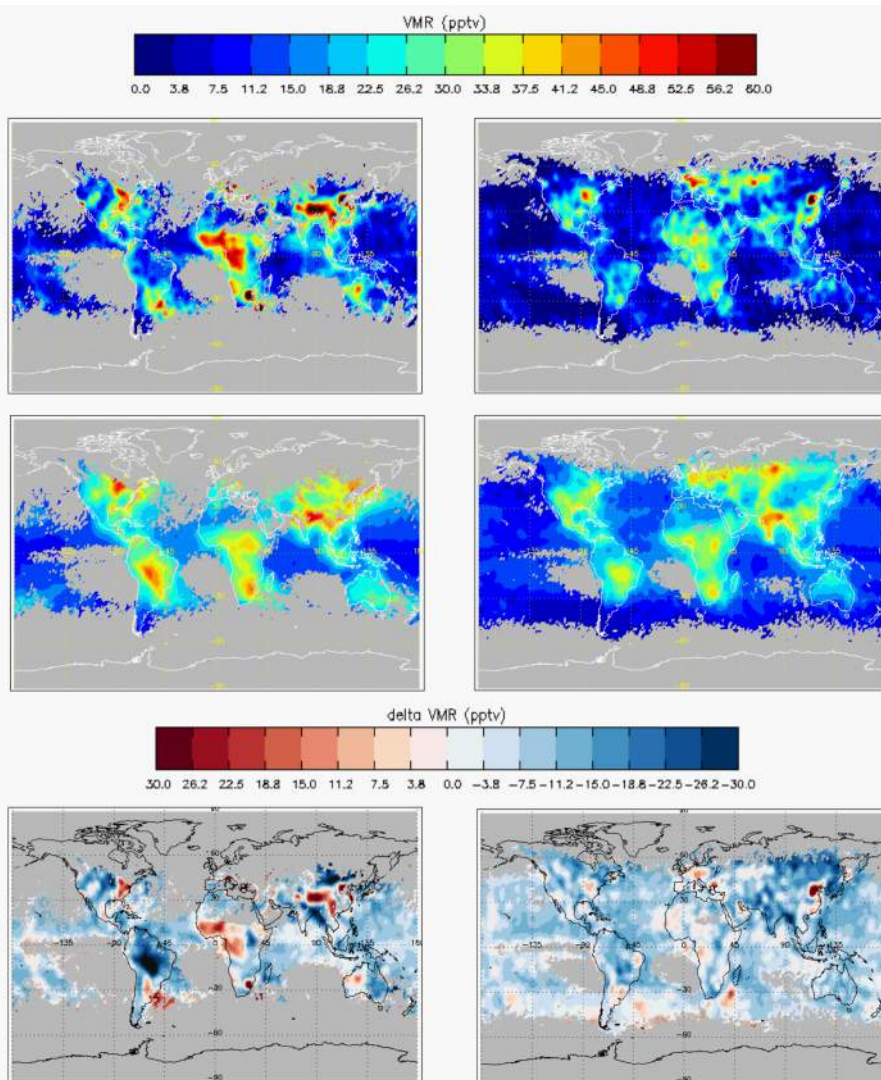
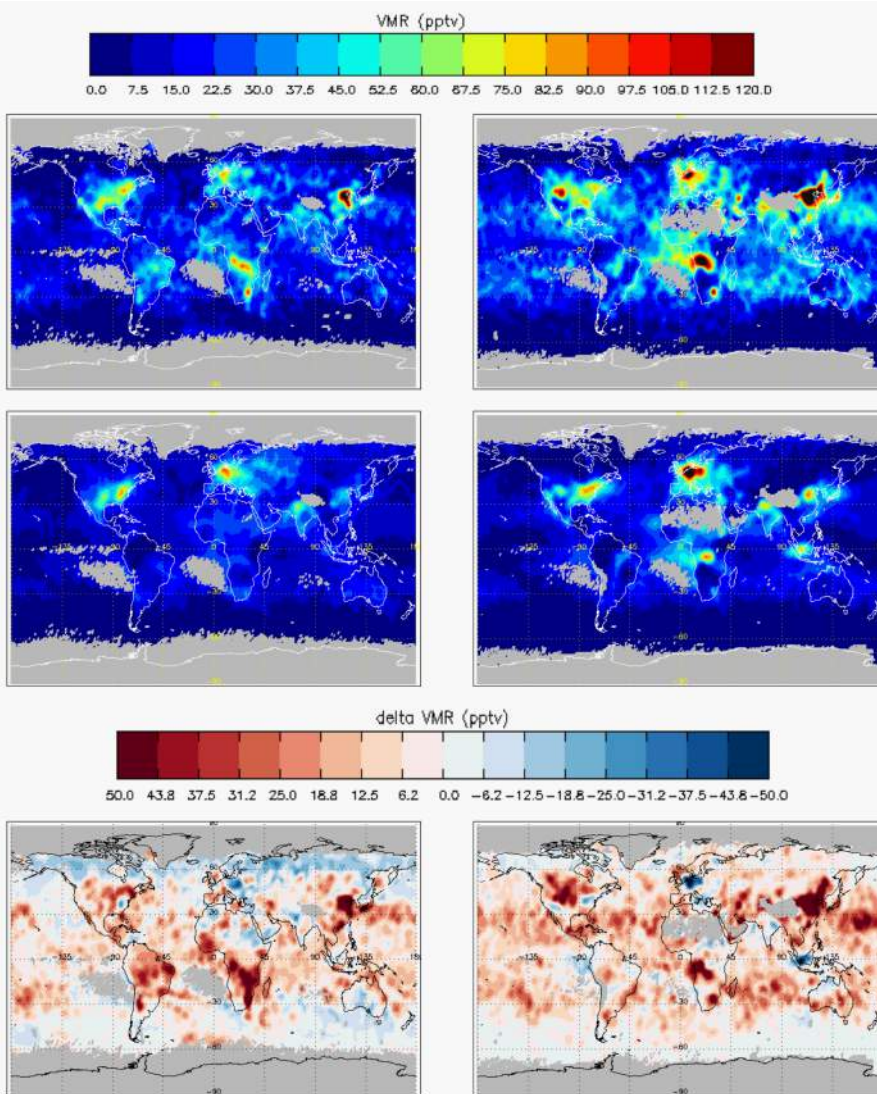
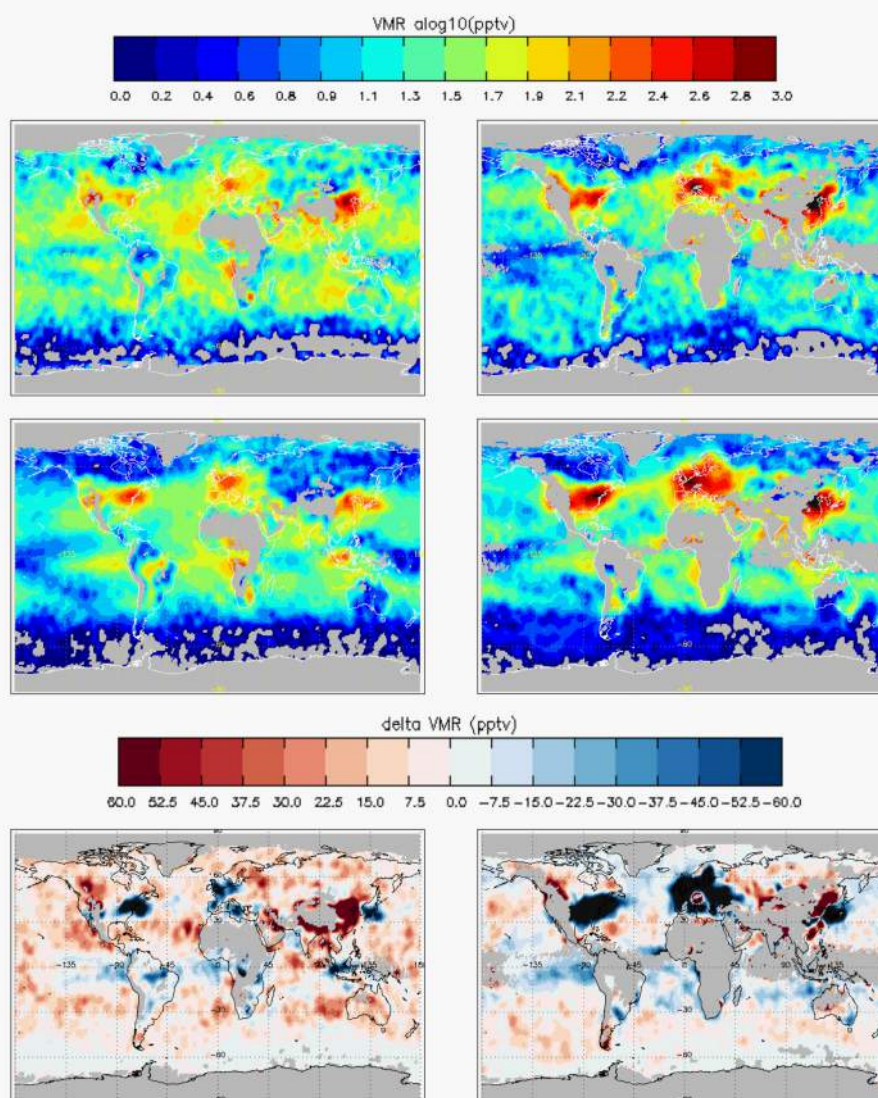


Figure 5a. Upper cloud levels (280 hPa left, 380 hPa right): OMI versus TM4 model NO₂ VMRs (OMI top, TM4 middle, difference bottom) average quantities for the year 2006.



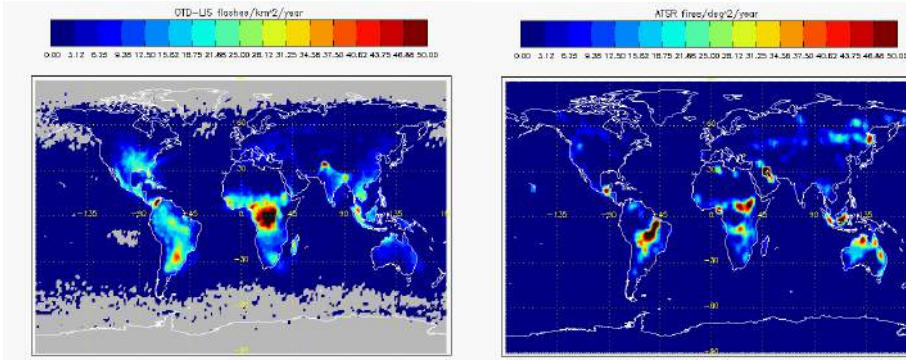
1
2 Figure 5b. Middle cloud levels (500 hPa left and 620 hPa right): OMI versus TM4 model NO₂
3 VMRs (OMI top, TM4 middle, difference bottom) average quantities for the year 2006.

4
Maria Belmonte Rivas 9/2/2015 3:03 PM
Deleted: (middle row, 500 and 620 hPa)



2
3 Figure 5c. Lower cloud levels (720 hPa left and 820 hPa right): OMI versus TM4 model NO₂
4 VMRs (OMI top, TM4 middle, difference bottom) average quantities for the year 2006.

Maria Belmonte Rivas 9/2/2015 3:06 PM
Deleted:
 Maria Belmonte Rivas 9/2/2015 3:06 PM
Deleted: : for low clouds (bottom row, 720 and 820 hPa)



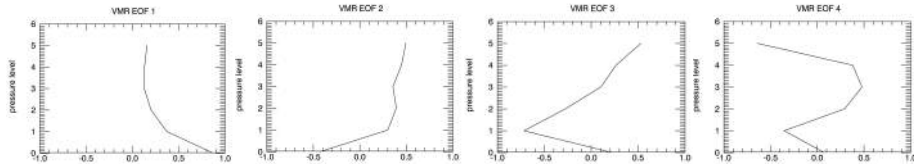
1

2 Figure 6. [Interpretation aids for process attribution: mean](#) flash rate climatology (1998-2010)
 3 from [the LIS-OTD sensor](#) (left, [Cecil et al., 2014]) and fire count [climatology](#) (1997-2003)
 4 from [the ATSR sensor](#) (right, [Arino et al., 2012]).

5

Maria Belmonte Rivas 9/2/2015 11:49 AM

Deleted: Mean



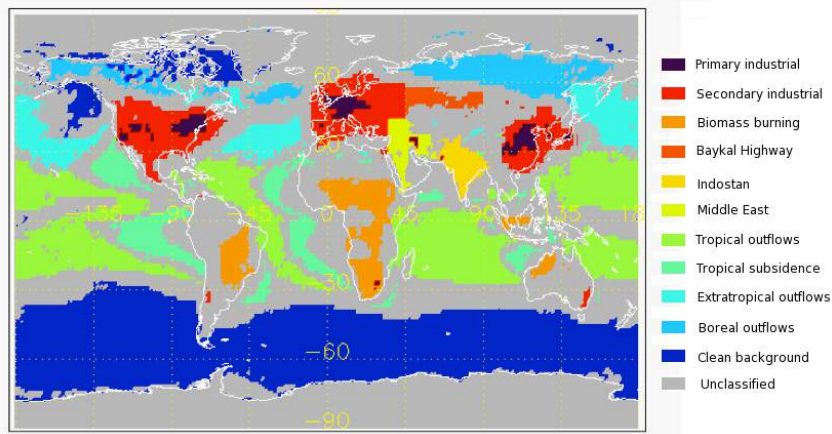
1

2 | Figure 7a. Classification EOFs: surface source, outflow, high/low outflow, middle outflow.

3

Maria Belmonte Rivas 9/2/2015 12:09 PM

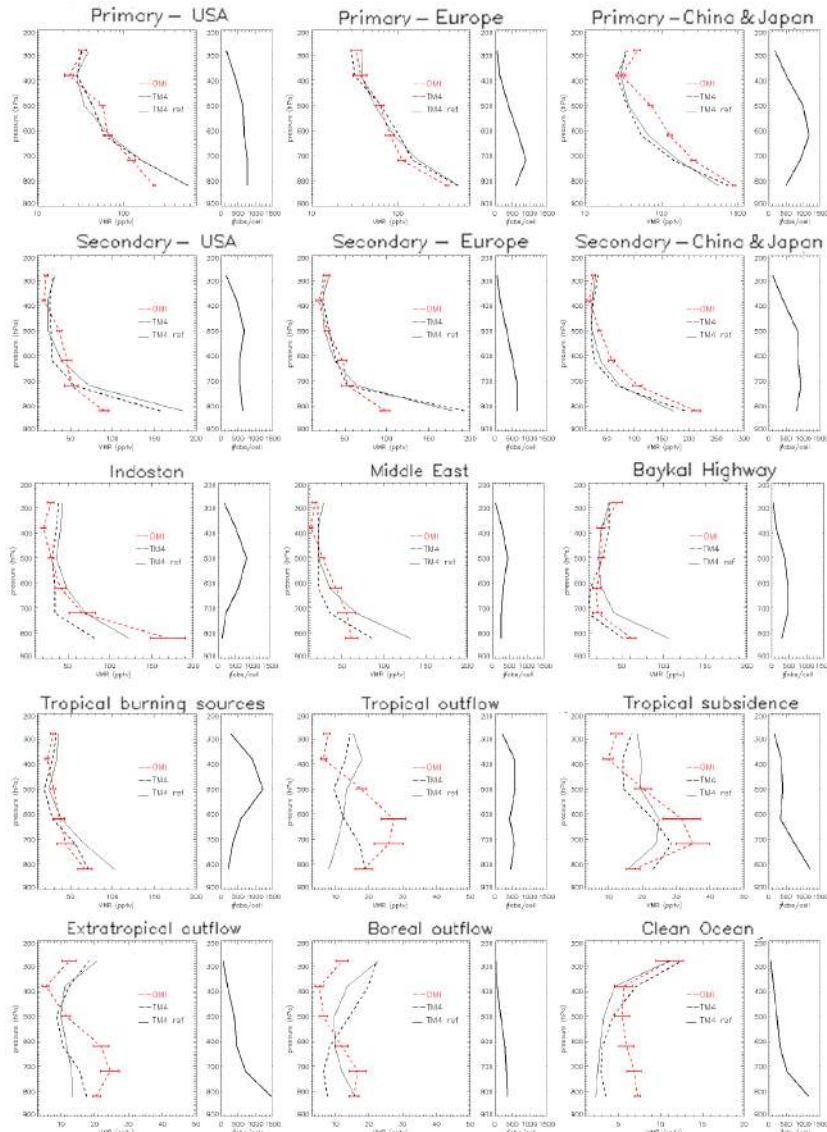
Deleted: (pumped/subsided)



4

5 | Figure 7b. Model based classes based on EOF decomposition of model NO₂ profiles under
6 | cloudy conditions: black (primary industrial), red (secondary industrial), orange (biomass
7 | burning), ochre (Baykal Highway), yellow (Indostan), light green (Middle East), green
8 | (tropical outflow), turquoise (tropical subsidence), cyan (extratropical outflow), blue (boreal
9 | outflow), dark blue (clear background). Gray for unclassified.

10

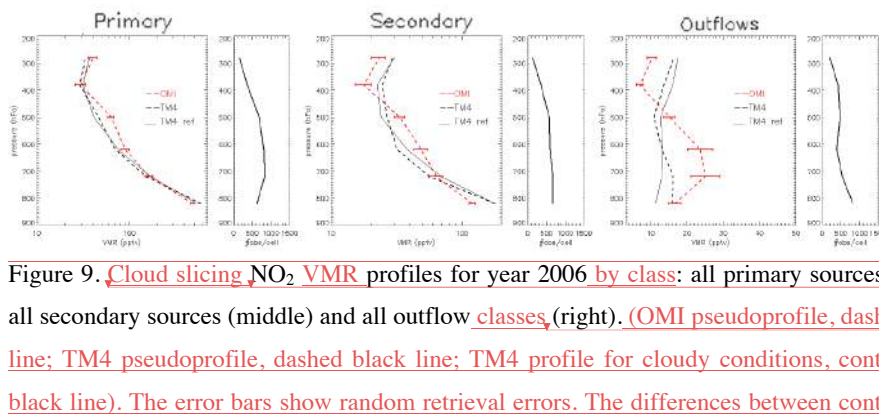


1

2 Figure 8. Cloud-slicing NO₂ VMR profiles for the year 2006 by class (OMI pseudoprofile,
3 dashed red line; TM4 pseudoprofile, dashed black line; TM4 profile for cloudy conditions,
4 continuous black line). The error bars show random retrieval errors. The differences between
5 continuous and dashed black lines show systematic pseudoprofile errors. The subpanels on
6 the right show the average number of OMI observations collected per grid cell per year for
7 that class.

Maria Belmonte Rivas 9/2/2015 12:42 PM
Deleted: Mean tropospheric

Maria Belmonte Rivas 9/2/2015 12:45 PM
Deleted: First row: Primary USA, Europe, China. Second row: Secondary USA, Europe, China. Third row: India, Middle East, Baykal Highway. Fourth row: tropical biomass burning, tropical outflows, tropical subsidence. Fifth row: extratropical outflow, boreal outflow, clean background.



2
3 Figure 9. Cloud slicing, NO₂ VMR profiles for year 2006 by class: all primary sources (left),
4 all secondary sources (middle) and all outflow classes (right). (OMI pseudoprofile, dashed red
5 line; TM4 pseudoprofile, dashed black line; TM4 profile for cloudy conditions, continuous
6 black line). The error bars show random retrieval errors. The differences between continuous
7 and dashed black lines show systematic pseudoprofile errors.

Maria Belmonte Rivas 9/2/2015 1:47 PM
Deleted: Average
 Maria Belmonte Rivas 9/2/2015 1:47 PM
Deleted: tropospheric
 Maria Belmonte Rivas 9/2/2015 2:39 PM
Deleted: s

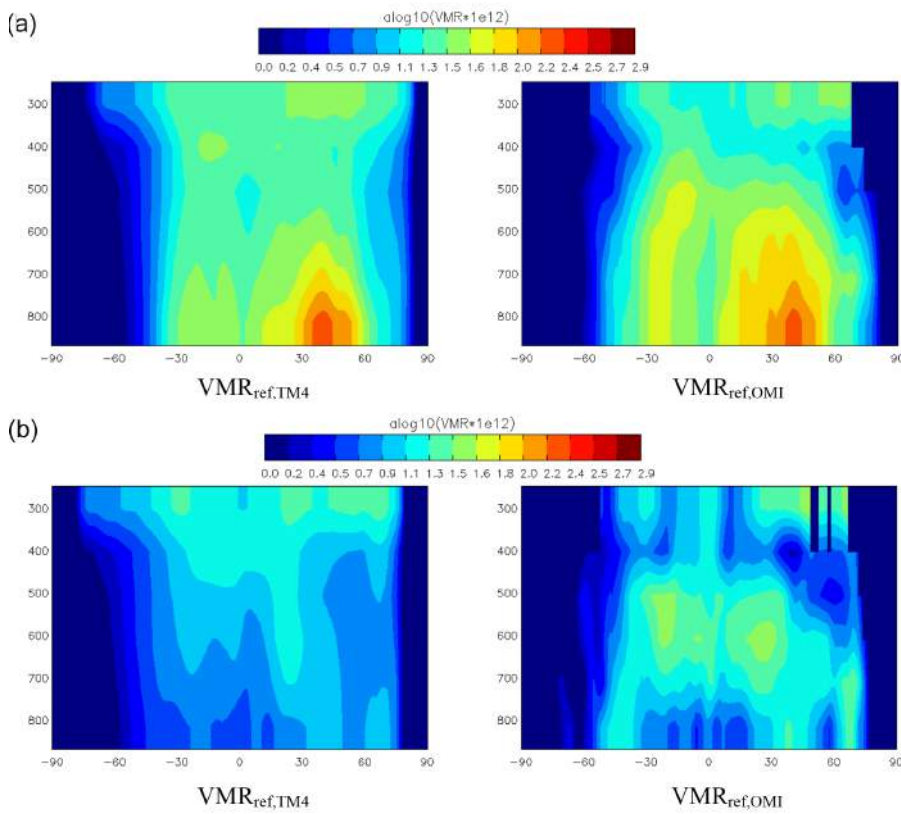


Figure 10a. Latitude-height cross-section of annual zonal mean tropospheric NO₂ from TM4 (left) and OMI (right) with CRF>50%.

Figure 10b. Latitude-height cross-section of annual zonal mean tropospheric NO₂ from TM4 (left) and OMI (right) with CRF>50% over the remote pacific sector (180W-135W).

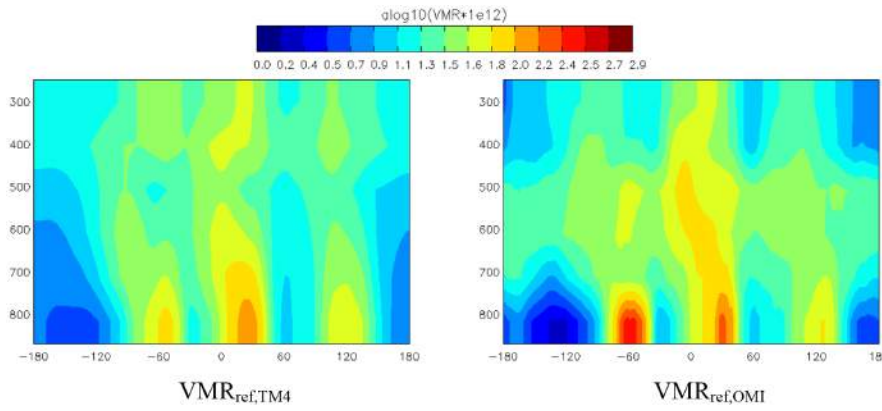


Figure 11. Longitudinal cross-section of annual mean tropospheric NO₂ from TM4 (left) and OMI (right) with CRF>50% over the tropics (10N-20S).

Maria Belmonte Rivas 9/2/2015 3:12 PM
Deleted: p

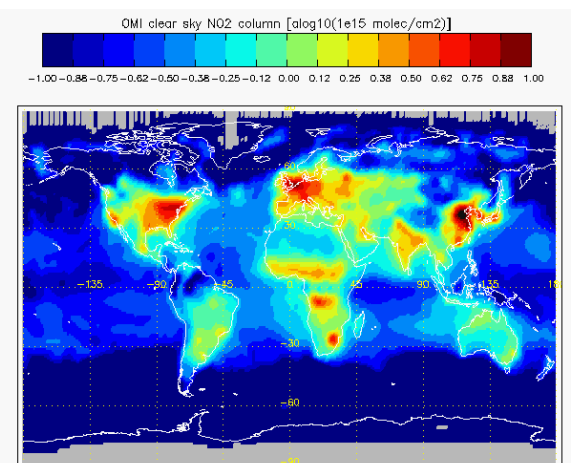
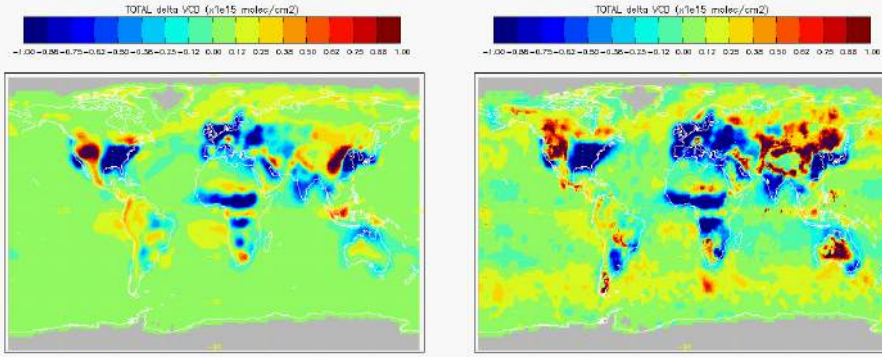


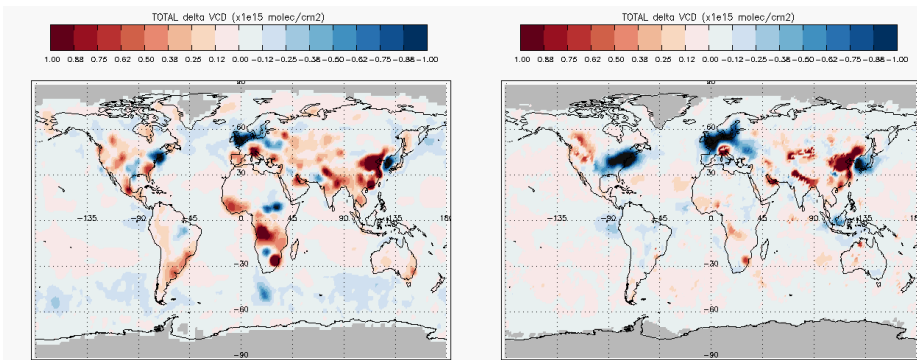
Figure 12. Annual clear sky OMI tropospheric NO₂ total columns for the year 2006.



1

2 Figure 13. Total tropospheric NO₂ columns differences between cloudy (CRF>50%) and clear
3 (CRF<25%) conditions for TM4 (left) and OMI (right).

4



5

6 Figure 14. Total tropospheric NO₂ column differences (OMI-TM4) in clear (left) and cloudy
7 (right) conditions for the year 2006.

8